Journal of Cellular Biochemistry 30:133–170 (1986)
Perspectives in Inflammation, Neoplasia, and Vascular Cell Biology 127–164

Molecular Mechanisms of Cytolysis by Complement and by Cytolytic Lymphocytes

Eckhard R. Podack

Department of Microbiology/Immunology, New York Medical College, Valhalla, New York 10595

Recent advances in our understanding of the mechanism of NK cell and cytolytic T-lymphocyte (CTL)-mediated cytolysis have revealed intriguing analogies of lymphocytic effector mechanisms with those of complement. Each of these cytolytic effector systems assembles on target membranes cytolytically active, tubular complexes from hydrophilic precursor proteins. Membrane insertion of the tubular complexes gives rise to ultrastructural membrane lesions and causes target cell lysis by disruption of the target membrane (Fig. 1). Assembly of tubular transmembrane complexes involves the polymerization of monomeric precursor proteins to transmembrane pores that serve to lyse cells directly and to permit entry of additional lytic factors. This review will summarize the molecular events resulting in the formation of membrane lesions by lymphocytes and by complement and our knowledge of additional cytolytic factors. It will become apparent that there are striking analogies in the morphology and function of the tubular complexes, their mode of assembly, as well as their utilization as transmembrane channels for entry of cytolytic factors.

ASSEMBLY OF THE MEMBRANE ATTACK COMPLEX (MAC) OF COMPLEMENT

Formation of the MAC proceeds in a stepwise assembly of five proteins to a complex with approximately 20 subunits. The assembly may be divided into two stages with regard to function, structure, and control: (1) The insertional event carried out by the trimolecular C5b-7 complex. This reaction proceeds without overt lysis but it sets the stage for subsequent membrane damage. (2) Membrane damage by binding of C8 and polymerization of C9 to the tubular transmembrane complex that is responsible for formation of the ultrastructural membrane lesion.

For the purpose of this review, the second stage, the formation of membrane lesions by polymerization of C9, will be described first because it exemplifies

Received March 20, 1985; revised and accepted September 25, 1985.

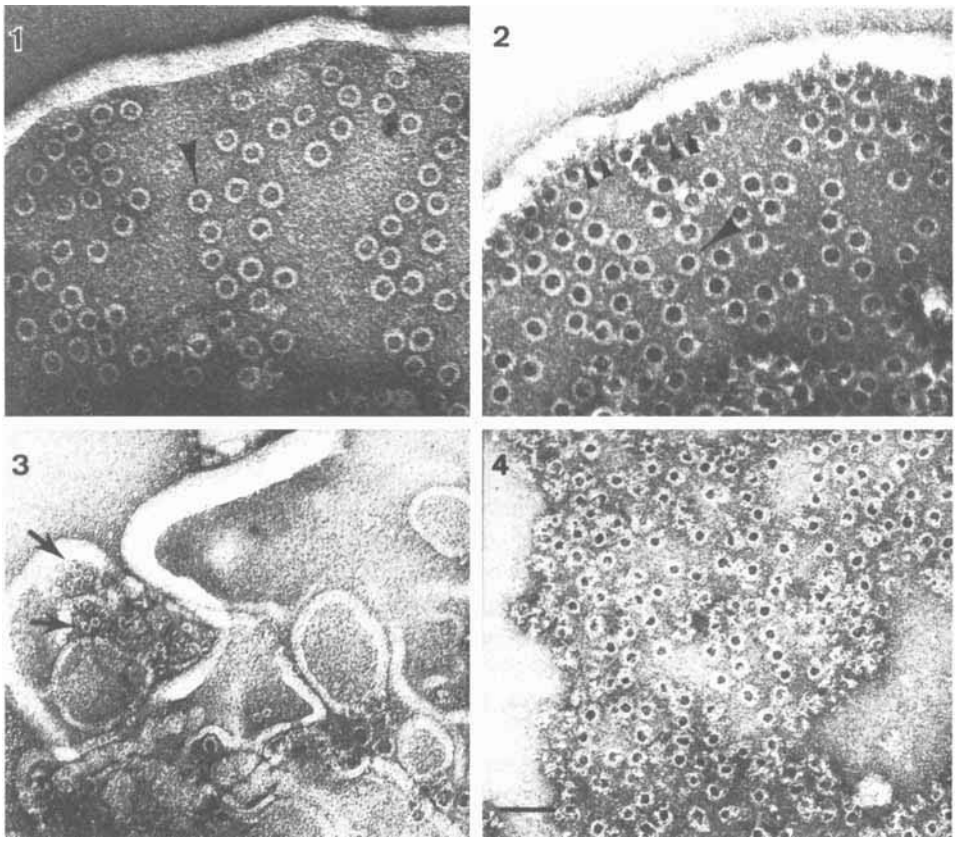

Fig. 1. Ultrastructural membrane lesions induced by CTL, NK cells, and complement. Panels 1 and 2) Poly perforin 1 (internal diameter 160 Å). Panel 3) Poly perforin 2 (internal diameter 50–70 Å) of murine CTL and NK cells. Panel 4) Human complement lesions. Scale bar: 640 Å.

principles for the transition of hydrophilic precursors to amphiphilic complexes that seem to be operative also in the insertional reaction in the first stage of assembly.

Polymerization of C9 to Tubular Complexes

Monomeric, purified C9, upon prolonged incubation at 37°C, polymerizes and assumes the structure of a 100 Å wide, hollow tubule of 160 Å length bearing a 200 Å wide torus on one end and a hydrophobic membrane combining site on the opposite end (Fig. 2) [1]. Polymerization is greatly accelerated in the presence of Zn ions [2] and, less dramatically, by Ca and Mg. Figure 2 shows the ultrastructure of polymerized C9 as determined by negative staining electron microscopy in comparison complement lesions (inset).

Heterogeneity of C9 Polymers and Their Physicochemical Stability

Polymeric C9 is heterogeneous owing to the presence of polymers with various subunit numbers and of open and completely closed tubules [3]. A significant increase in the stability of poly C9 is observed after circular polymerization and complete

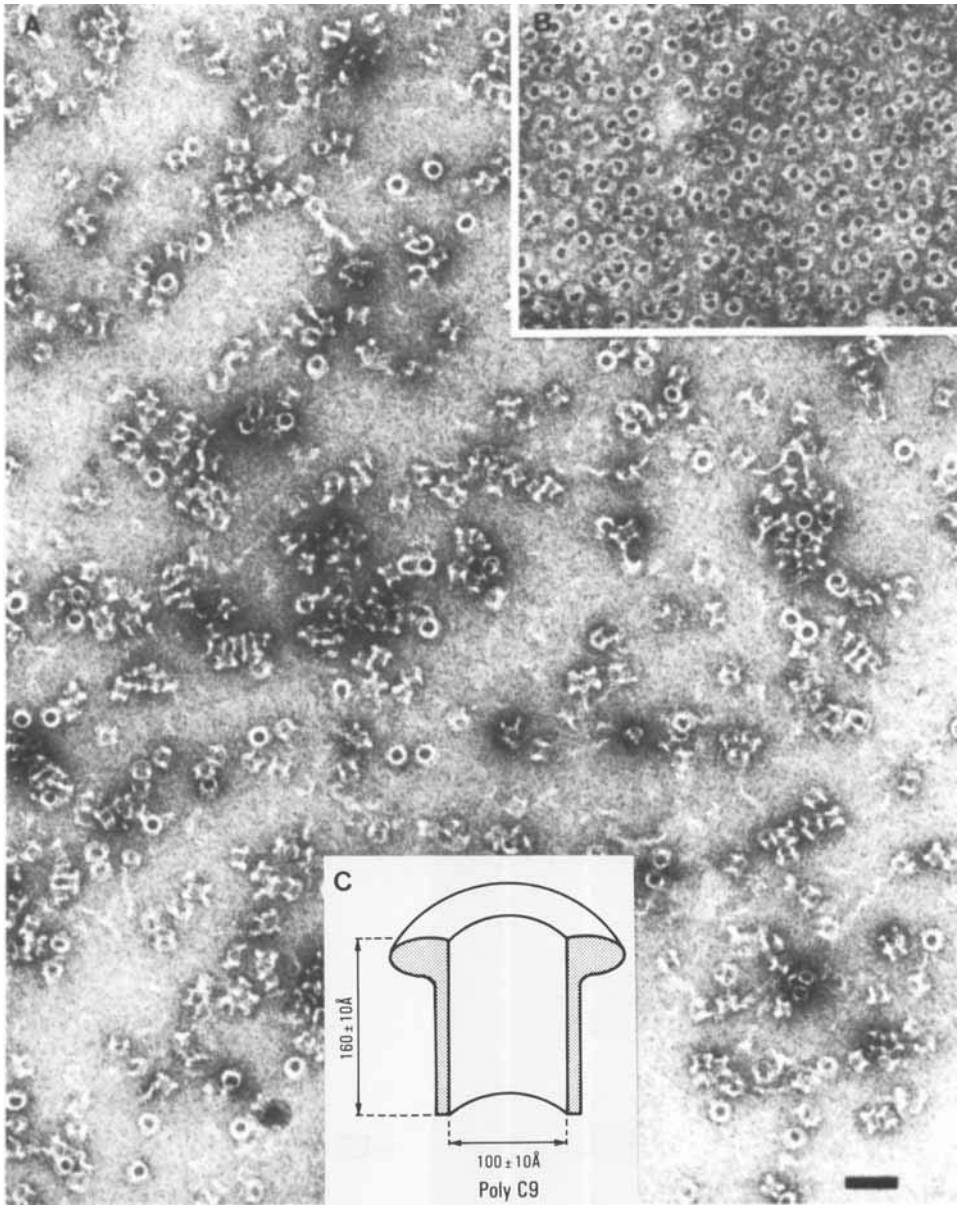

Fig. 2. Ultrastructure of poly C9 (main panel) in fluid phase in comparison to complement membrane lesions (inset, upper right). The inset in the lower part of the figure shows a schematic view of poly C9 bisected along its vertical tubular axis.

closure of the poly C9 tubule. (This form of poly C9 is designated tubular poly C9 [t-poly C9] as opposed to nontubular [nt] poly C9.) The closed tubule of t-poly C9 is resistant to dissociation by boiling in sodium dodecyl sulfate (SDS) even under reducing conditions and migrates in SDS polyacrylamide gels as a protein with an apparent molecular weight of 1.1×10^6 (Fig. 3, left two tracks). Polymers of C9 not composed of complete tubules (nt-poly C9), in contrast, are dissociated by SDS even under nonreducing conditions and migrate as monomeric C9 upon sodium dodecyl sulfate-polyacrylamide gel electrophoresis (SDS-PAGE). To dissociate tubular poly C9, it is necessary to treat the complex with 6 M guanidine isothiocyanate for several hours at 60°C or to boil the complex with SDS in the presence of 8 M urea for 10–15 min. Dissociation under those conditions ensues in the absence of reducing agents, indicating strong noncovalent subunit interactions [3].

C9 subunits in poly C9 can also be covalently linked by a spontaneous disulfide exchange reaction between adjacent subunits in the poly C9 tubule [4–6]. This disulfide exchange reaction is greatly accelerated by the addition to poly C9 of low concentrations of free sulfhydryl reagents.

Tubular poly C9 is resistant to proteolytic degradation, whereas nt-poly C9 is completely digested to small peptides that dissociate in the presence of SDS [3]. Trypsin cleaves a fragment off t-poly C9 and reduces the apparent molecular weight of the complex from 1.1×10^6 to approximately 800,000. The fragment probably is

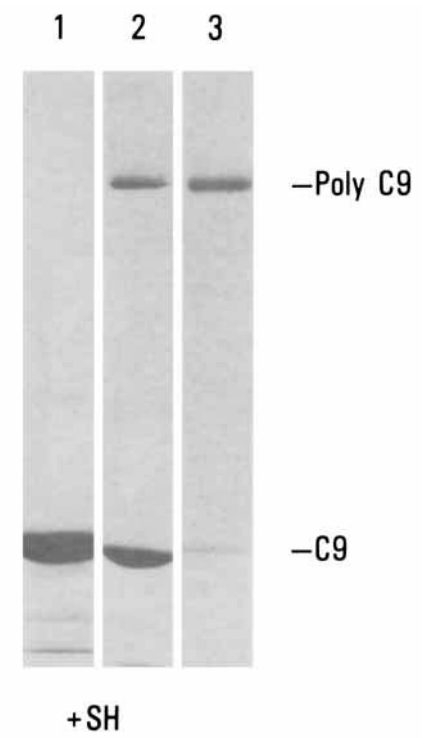

Fig. 3. SDS-polyacrylamide gel analysis of monomeric C9 (left), polymerized C9 containing t-poly C9 and nt-poly C9 (middle), and homogeneous t-poly C9 (right). The electron micrograph of Figure 2 was obtained with material in the middle track.

derived from the poly C9 torus because the ultrastructure of trypsinized poly C9 is a 170 Å long tubule lacking the torus [3]. Figure 4 shows the electron micrographs and schematic drawings of the ultrastructural comparison of tubular poly C9 after boiling in SDS and after trypsinization. The tubular wall remains intact, whereas the peptide chain that forms the torus is unfolded by SDS and removed by trypsin. The functional significance of the unusual stability of poly C9 lies in its resistance to physical or chemical degradation by target defense mechanisms after insertion as cytolytic transmembrane channel into target membranes.

Molecular Weight of Tubular Poly C9

SDS-resistant t-poly C9 can be separated from nt-poly C9 after boiling in SDS by gel-filtration and sucrose density gradient ultracentrifugation [3] and obtained in homogenous form free of other polymers (see Fig. 3, track 3). The mean molecular weight of t-poly C9 purified in this way is $1.1 \times 10^6 \pm 150{,}000$ (SD) as determined by SDS-PAGE, sedimentation equilibrium analysis, and electron scattering in the scanning transmission electron microscope (Table I) [7]. All methods indicate a range of 11 to 20 C9 protomers per poly C9 tubule in a Gaussian distribution. Approximately 75% of the tubules contain 14 to 16 C9 monomers. Figure 5 shows the image of t-poly C9 containing 17 protomers as suggested from image enhancement by rotational autocorrelation analysis (courtesy Dr. R. Guckenberger, Max Planck Inst. f. Biochemistry, Martinsried, FRG). This method also showed complexes with various subunit numbers ranging from 12 to 18.

Hydrophilic Amphiphilic Transition of C9 During Polymerization and Formation of Functional Transmembrane Channels

Polymerization of C9 in the presence of single bilayer phospholipid vesicles results in the membrane insertion of poly C9 tubules and in the release of membrane

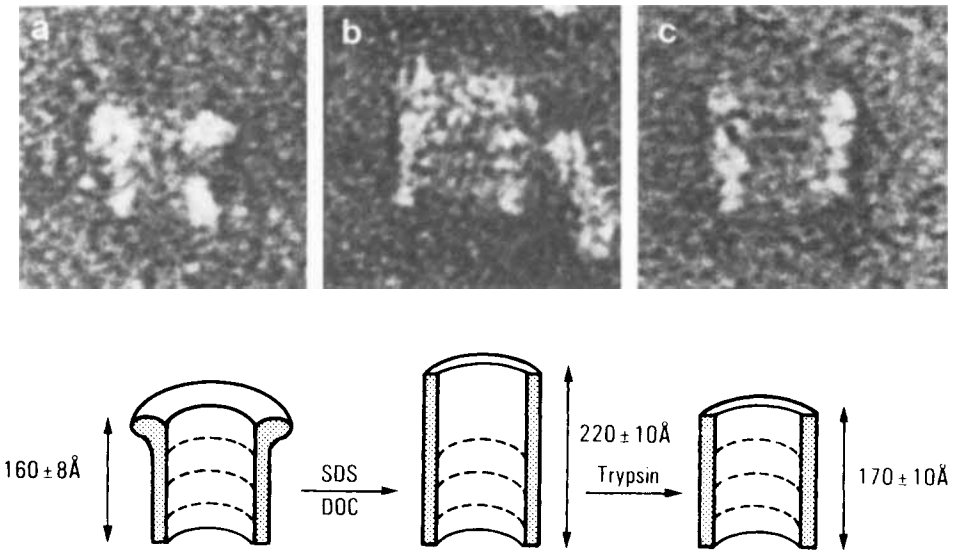

Fig. 4. Ultrastructure of poly C9 (a), poly C9 after boiling in SDS (b), and poly C9 after treatment with a tenfold molar excess of trypsin (c). The lower panels show the same complexes in schematic form.

TABLE I. Molecular Weight of 27 S poly C9

Method	Molecular wt (mean ± SD)	No. of C9 subunits per poly C9 tubule (observed range)[a]
SDS-PAGE	$1.1 \times 10^6 \pm 150{,}000$	13–17
Sedimentation equilibrium	$1.09 \times 10^6 \pm 118{,}000$[b]	12–18
Scanning transmission electron microscope	$1.078 \times 10^6 \pm 194{,}000$	11–20

[a]Subunit number calculated assuming Mr 71,000 for monomeric C9.
[b]Value corrected for detergent binding of 0.27 g DOC/g poly C9 or 0.54 g SDS/g poly C9, respectively.

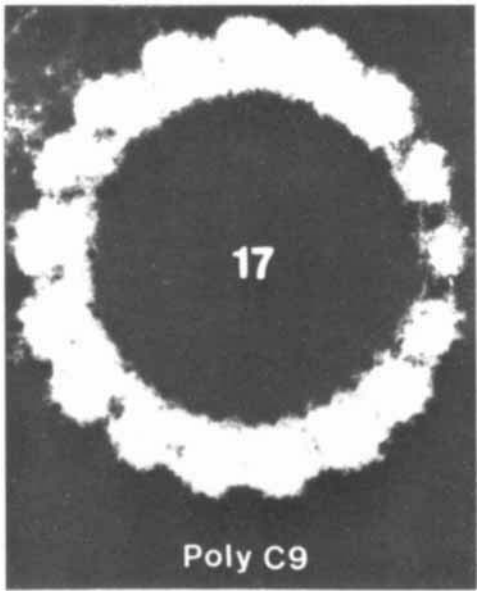

Fig. 5. Image-enhanced poly C9 containing 17 protomers (in collaboration with Dr. R. Guckenberger, Max Planck Inst. f. Biochemistry, Martinsried, Germany).

entrapped markers [8] (Fig. 6). Poly C9 tubules penetrate 40 Å deep into the phospholipid bilayer. 120 Å of the poly C9 tubule bearing the torus projects above the membrane surface. This suggests the presence of a 40 Å long, hydrophobic domain on the end of poly C9 opposite to the torus. This domain aggregates poly C9 complexes in fluid phase (see Fig. 2), resulting in 40 Å overlapping, side-by-side aggregates of poly C9 in which the tori of adjacent complexes point in opposite directions.

When C9, during polymerization, inserts into a planar lipid bilayer separating two voltage clamped buffer chambers, discrete step conductance increases are observed with a wide distribution in size and a median of 6 nS/channel in 0.1 M NaCl at pH 7.0 [9]. Insertion of preassembled homogeneous t-poly C9 by osmotic fusion or with detergents into planar membranes causes the formation of large, voltage-independent transmembrane channels of larger diameter with a narrower range of sizes averaging 70–80 nS. Using a 160 Å long, hollow tubule as the basis for

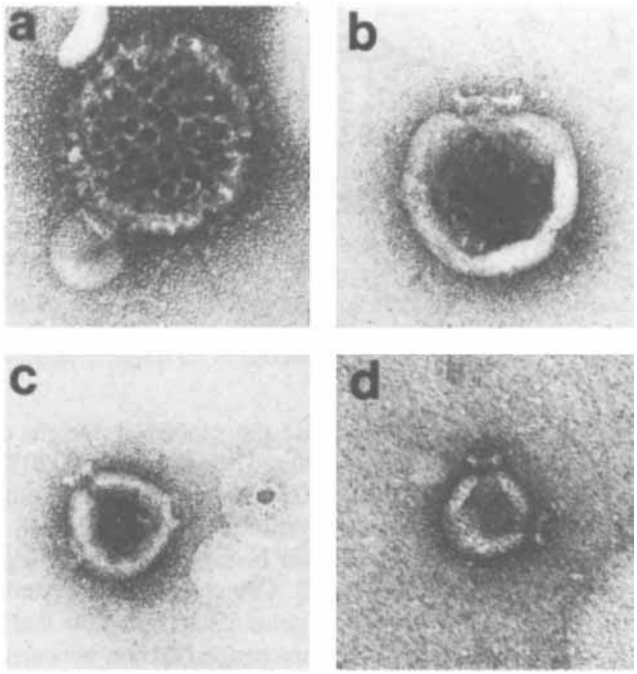

Fig. 6. Poly C9 inserted into single bilayer vesicles. a) Numerous poly C9 tubules per vesicle seen in top and side view. b) Two adjacent poly C9 tubules in the side view (and several faintly visible in top view). c) Side and top view of poly C9. d) Two poly C9 tubules in side view. Note stain penetration into all vesicles.

calculating the functional pore size of t-poly C9 from the conductance increase, a channel of approximately 70 Å is estimated [9]. This functional pore size approaches the structural size of the poly C9 channel, as seen by electron microscopy, and represents the first direct correlation of the functional pore size effected by a structurally well-defined complex in complement.

Restricted Unfolding of Monomeric C9 During Polymerization

The dimensions of monomeric C9 in the electron microscope correspond to a globular protein with axes of 50 Å and 80 Å lengths [1]. This value agrees with the hydrodynamic properties of C9. In poly C9 the length of C9 protomers is a 160 Å, implying an unfolding of C9 during polymerization. Unfolding probably is induced by high-affinity association of C9 monomers and may be responsible for the exposure of previously hidden hydrophobic domains (Fig. 7) [1]. Unfolding of C9 is accompanied by an increase in β-structure [8], increased acidity, and expression of neoantigenic sites [10] in poly C9. These observations suggest a drastic conformational rearrangement of C9 during polymerization and transmembrane channel formation as shown in Figure 7.

Primary Structure of C9

The sequence of C9 has been deduced from the nucleotide sequence of cDNA clones coding for C9 (Fig. 8) [11]. The C9 peptide chain has 537 amino acids with a

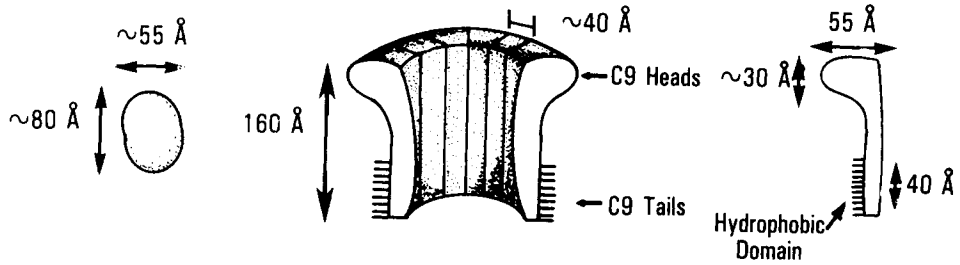

Fig. 7. Hypothetical model for C9 unfolding during polymerization. Left panel) Monomeric C9. Middle) Poly C9. Right) Putative structure of unfolded C9 protomers. The hydrophobic domain in poly C9 is indicated by parallel lines, which would correspond to the length of insertion of poly C9 into membranes.

molecular weight of 60,700 (Fig. 8). Since the molecular weight of intact C9 is 73,000 by sedimentation equilibrium analysis [7], approximately 20% of C9's mass consists of carbohydrate. The sequence of C9 shows two clusters of cystein residues in the C9a domain and the C9b domain, respectively (underlined in Fig. 8). These domains are not disulfide-linked to each other because they can be separated without reduction after thrombin cleavage of C9 [15]. C9b contains eight cystein residues and C9a (the N-terminal thrombin fragment) contains 15. It is possible that the odd cystein residue of C9a is involved in the disulfide-exchange reaction between C9 protomers observed in poly C9. In addition, it may be speculated that the peptide sequence around the thrombin cleavage site serves as a hinge allowing the restricted unfolding of globular C9 to the extended amphiphilic molecule during polymerization. The C9 sequence published by Stanley et al [13] containing an even number of cystein residues and a threonine instead of proline at position 395 may suggest C9 polymorphism.

The linear sequence of C9 does not show any extended hydrophobic amino acid sequence. A hydrophobicity plot [11] reveals that the C9b domain overall is more hydrophobic than C9a. Photolabeling studies with membrane-restricted probes showed that the C9b domain of membrane-inserted poly C9 is in contact with the hydrophobic interior of membranes [12]. The C9a sequence is 35% homologous in position 72–111 with the sequence of the LDL receptor [11,13,14]. This sequence contains six conserved cystein residues that are likely to serve in the stabilization of the C9a domain (Fig. 9).

Mechanisms of C9 Polymerization

The detailed mechanism of C9 polymerization is not known; however, several intriguing observations relating to a possible mechanism have been made.

Effect of detergents. Incubation of monomeric C9 with sodium deoxycholate, octylglucoside, or NP40 causes rapid C9 polymerization. C9 polymers formed by this procedure are largely nontubular and can be recombined with phospholipids by the detergent dialysis or gel-filtration procedure. C9 polymers generated with detergents, therefore, are amphiphilic [1].

Chaotropic agents. Guanidine HCl (1 M) causes rapid C9 polymerization to long, linear C9 polymers that do not exhibit hydrophobicity. Guanidine-polymerized C9 (1 M) dissociates to C9 monomers in 4 M guanidine and regains lytic activity upon removal of the chaotrope by dialysis at 4°C [1].

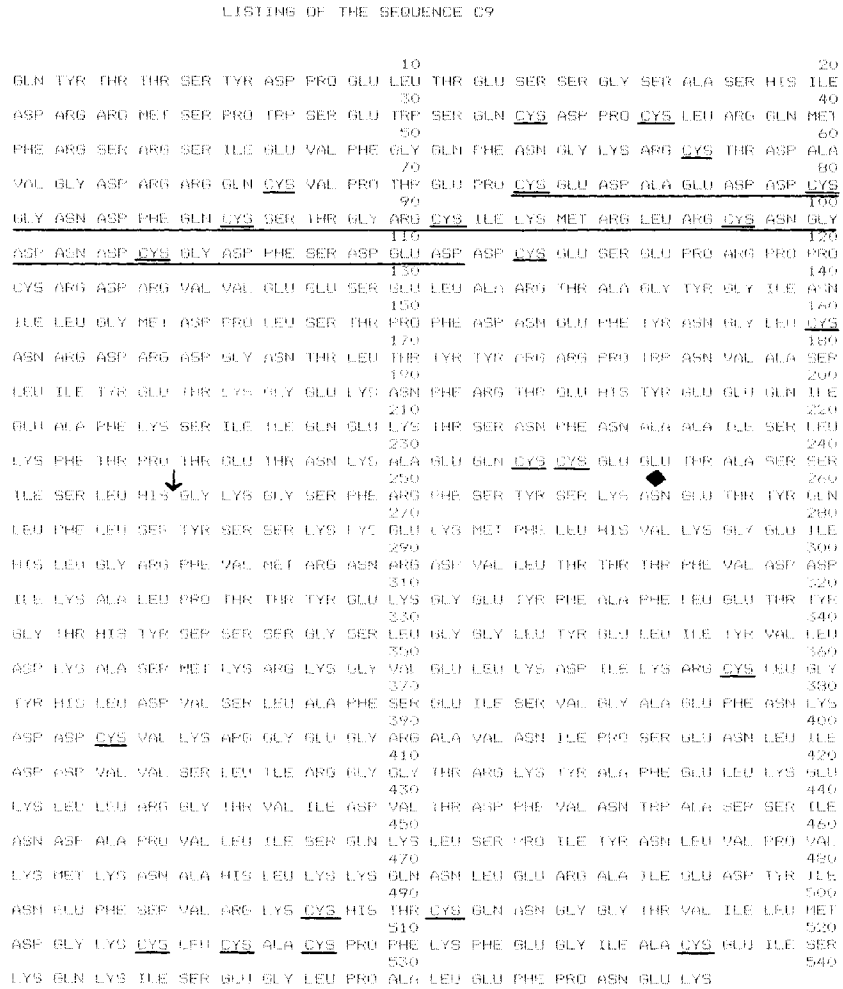

Fig. 8. Derived amino acid sequence of C9. Cystein residues are underlind. The arrow indicates the position of the thrombin cleavage site; the diamond marks a putative glycosylation side. The underlined portion is the sequence that is homologous to the LDL receptor (see Fig. 9).

Heat. Increased temperature (42°C to 45°C) rapidly polymerizes C9 to a mixture of t- and nt-poly C9. The ratio of nt-poly C9 increases with increased temperature. Below 30°C no C9 polymerization is observed, even after very long incubation periods [1,8].

Metal ions and ionic strength. Zn ions at an equal molar ratio to C9 accelerate C9 polymerization at 37°C from 64 hr in the absence of Zn to 2–3 hr in its presence [2]. Other bivalent metal ions such as Ca and Mg have some effect on the rate of polymerization also. C9 polymerization at normal ionic strength in the presence of Zn requires a 37°C temperature. At 1/10 normal ionic strengths, C9 polymerizes even at room temperature in the presence of Zn. Metal-induced C9 polymers contain the usual mixture of nt- and t-poly C9 and are indistinguishable ultrastructurally from poly C9 formed without added metals.

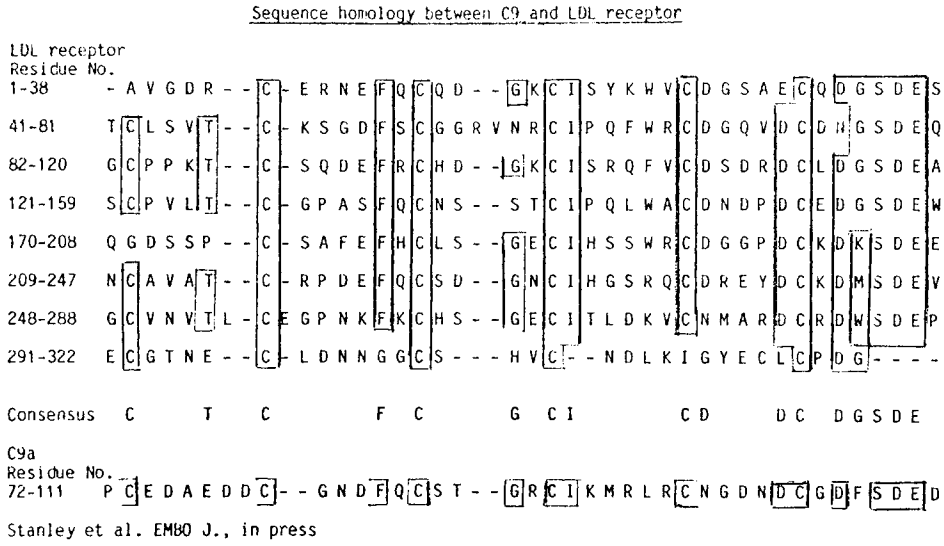

Fig. 9. Alignment of sequence homology between part of C9 and part of the LDL receptor.

Proteolytic enzymes. Thrombin-cleaved C9 fragments remain noncovalently associated and C9's activity is not altered [15]. Polymeric C9 formed with thrombin-cleaved C9 (C9 thro) contains a larger proportion of nt-poly C9, and the rate of polymerization of C9 thro is increased compared to uncleaved C9.

Limited trypsin digestion of monomeric C9 results in initial cleavage of an approximately Mr 20,000 fragment that remains noncovalently associated with C9 [3,15]. C9 try is more lytically active than intact C9 [Podack, unpublished] and its rate of tubular polymerization is also increased.

C5b-8 complex. C5b-8 rapidly polymerizes C9 at 37°C, and the forming poly C9 complex becomes tightly associated with C5b-8 to form the membrane attack complex (MAC) (see below). C5b-8 is the most efficient polymerizing agent known for C9 [10]. Reduction of poly C9 with low concentrations of DDT blocks hemolytic activity and polymerization by C5b-8.

The inducers of C9 polymerization may be categorized as in Table II. From inspection of this table, it appears that agents that perturb the tertiary structure or increase the flexibility of the peptide backbone or provide for increased C9-C9 contact may cause accelerated C9 polymerization. It is probable that the initial unfolding of one C9 molecule by any of the agents in Table II provides the nucleus for the formation of one tubule. This model suggests that an unfolded C9 molecule has a high affinity for monomeric, globular C9 and that the contact between the two molecules causes unfolding of globular C9 simultaneous with tight C9-C9 association and membrane insertion if the reaction occurs on a membrane surface. This chain reaction continues until the C9 tubule is closed or until the monomeric, globular C9 pool is exhausted. Reactions that perturb the tertiary structure of C9 to a larger extent may give rise to increased amounts of linear, noncircular C9 polymers.

TABLE II. Agents Causing C9 Polymerization

Agent	Presumed mechanism	Type of C9 polymer[a]	Remark
Detergents	Effect on tertiary structure, binding to hydrophobic crevices	Mostly nt-poly C9	
Chaotropes	Effect of tertiary structure	Linear poly C9	Polymers hydrophilic, not unfolded?
Heat	Effect on tertiary structure	Increased nt-poly C9 at increased temperature	
Metal ions	Increased C9-C9 contact	t-poly C9 and nt-poly C9	
Decreased ionic strength	Increased C9-C9 contact	t-poly and nt-poly C9	Polymerization at room temperature in presence of Zn
Proteolytic enzymes	Increased peptide backbone flexibility	t- and nt-poly C9	
C5b-8	C9-like structure?	t- and nt-poly C9	Physiological C9-polymerase

[a]C9 polymers are categorized as t- and nt-poly C9 (see text). In nt-poly C9 the tubules are not closed. Linear poly C9 shows little curvature and little tendency to form ring structures.

Polymerization of C9 by C5b-8: Formation of the Membrane Attack Complex

The C5b-8 complex is the physiological accelerator of C9 polymerization. Under similar conditions (normal ionic strength and pH at 37°C), spontaneous C9 polymerization requires 2–3 days, Zn-mediated polymerization requires 2–3 hr, and C5b-8-mediated polymerization requires 2–3 min. In addition to accelerating tubular C9 polymerization, C5b-8 directs the site of poly C9 insertion to its own binding site and facilitates C9's insertion into natural membranes into which C9 alone cannot insert even during polymerization. The mechanism by which C5b-8 induces C9 polymerization is not known. Free C8 has affinity for free C9 [10] and the two proteins form a stoichiometric, reversible complex at low ionic strength. It is probable that C5b-8 also has a single C9 binding site of higher affinity for C9 than monomeric C8. Interaction of C9 with this site may induce the unfolding of C9 and set into motion the chain reaction leading to a tubular poly C9 complex (Fig. 10). How the C9 unfolding by C5b-8 is achieved is a matter of speculation. Since C5b-8 has hydrophobic sites it may in some way resemble detergent-mediated C9 polymerization; alternatively, C9 binding to C5b-8 may perturb its tertiary structure sufficiently to cause its unfolding; the possibility has not been excluded that C5b-8 has enzymatic activity and causes cleavage of the one, initially interacting C9 molecule, thus facilitating its unfolding. The author's working hypothesis is that C5b-8 imitates an activated (unfolded) C9 molecule and provides a nucleation site for tubule formation just like an unfolded C9 molecule does. This model implies polymerization by physical association without covalent modification of C9. It also implies homologies between C5b-8 peptides and C9.

Composition of the MAC Tubule: The Transmembrane Channel of the MAC Is a Heteropolymer of C6, C7, C8 α-γ, and Poly C9

If C5b-8 imitates an activated C9 molecule causing C9 polymerization analogously to spontaneous C9 polymerization, then the interactions between C5b-8 and

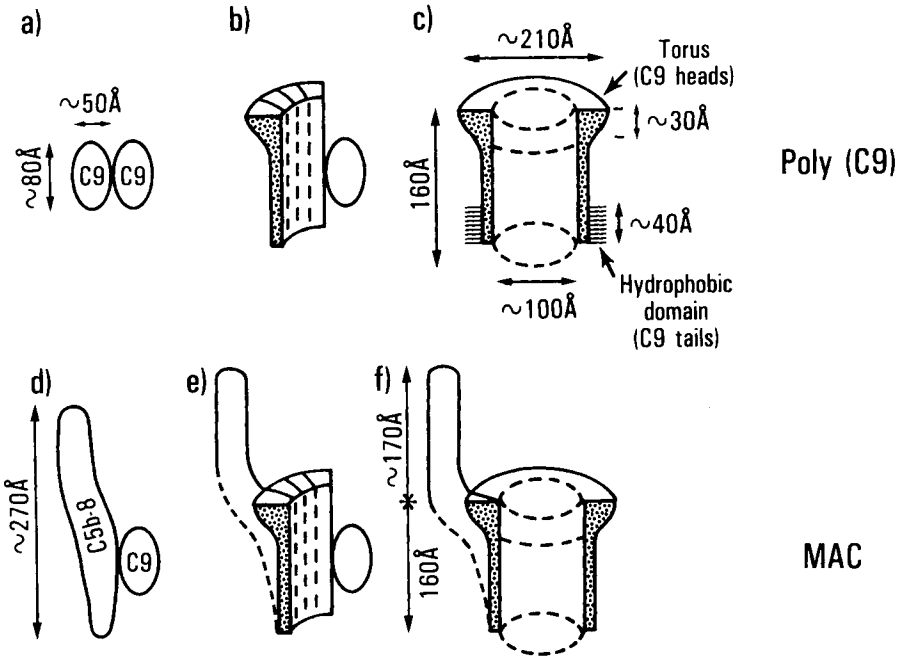

Fig. 10. Schematic drawing of spontaneous (a–c) and C5b-8-mediated C9 polymerization (d–f).

polymerized C9 should be as tight as C9-C9 interactions. The interaction of C5b-8 with C9 in the MAC tubule in fact is very strong and SDS resistant. The MAC thus is best defined as a fusion product of C5b-8 with poly C9 [C5b-8 (poly C9)]. The ultrastructure of the MAC in comparison to poly C9 is shown in Figures 10 and 11 in schematic form and in electron micrographs, respectively. The MAC contains an appendage on the poly C9 torus that has been identified as C5b-8 (arrows in Fig. 11, panels 4–6). The poly C9 portion (ie, the tubular part) of the MAC has all the characteristic properties of isolated poly C9, ie, increased β-structure, neoantigens, tubular ultrastructure, and resistance to dissociation by SDS [16,17]. Further analysis of the SDS-resistant tubular part of the MAC (designated MAC-poly C9) by various procedures revealed that it contained, in addition to 10–16 C9 molecules, one molecule of C6, one molecule of C7, and one molecule of C8α-γ. The subunits of C5b and C8β are not part of the SDS-resistant MAC-poly C9 tubule. Boiling of the MAC in SDS removes the appendage of C5b-8 along with the subunits of C5b and C8β (Fig. 12), whereas the tubular structure (MAC-poly C9) remains intact. The ultrastructure of SDS-resistant MAC-poly C9 is identical within the limits of resolution by negative staining electron microscopy to that of SDS-resistant poly C9, suggesting that C6, C7, and C8α-γ within MAC-poly C9 are in a similar conformation as C9 protomers. The proposed subunit arrangement in the MAC is shown in Figure 13. The transmembrane tubule of the MAC is composed of 10–16 C9 molecules with the participation of one molecule each of C6, C7, and C8α-γ, whereas the appendage consists of C5b and C8β. The precise arrangements of subunits within the two principal areas of the MAC await further studies. Initial efforts to demonstrate contact between C8 and C9 by cross-linking experiments have been negative [18]. Whether

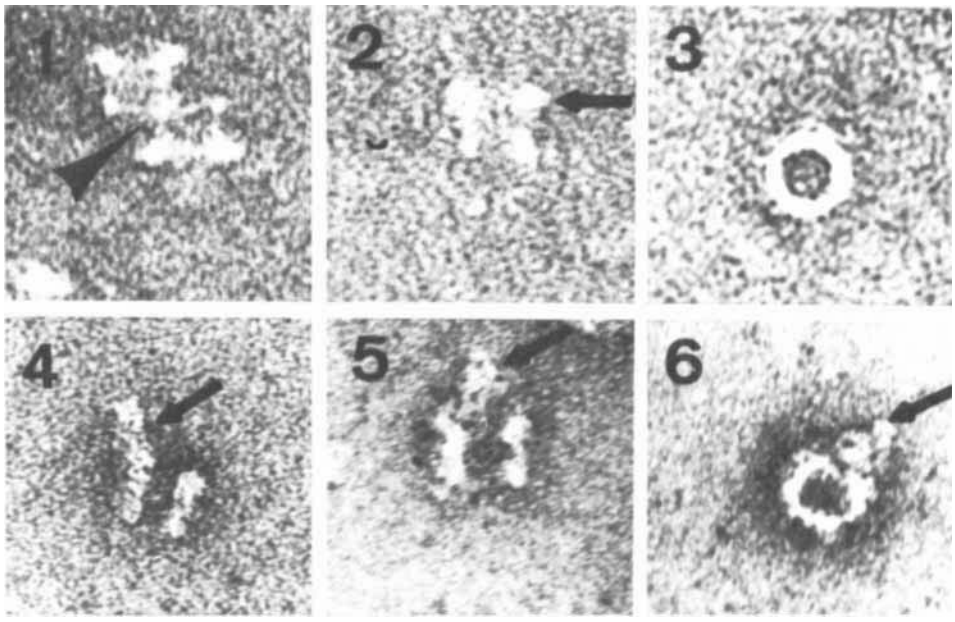

Fig. 11. Ultrastructure of poly C9 (panels 1–3) in comparison to the MAC (panels 4–6). Arrow in panel 1) Hydrophobic sites aggregating; two poly C9 complexes. Arrow in panel 2) Poly C9 torus. Arrows in panels 4–6) C5b-8 appendage in the MAC (lateral, frontal, and top view).

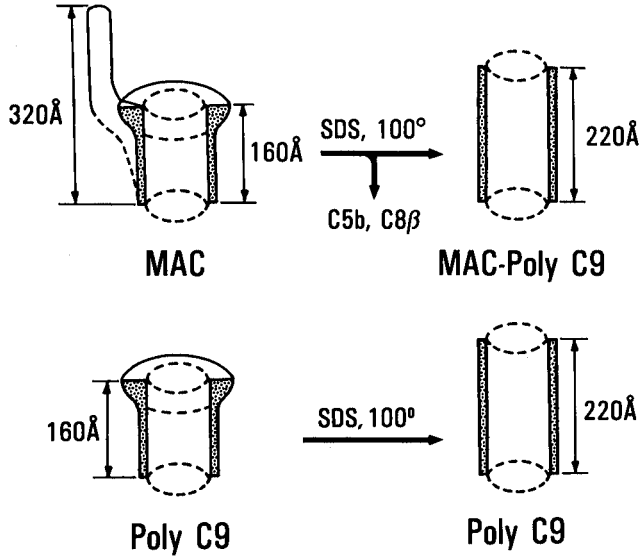

Fig. 12. Effect of boiling in SDS on the structure of the MAC and poly C9.

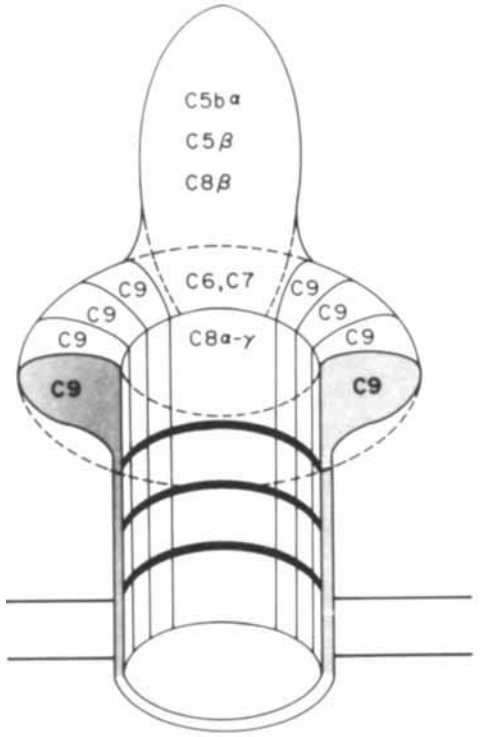

Fig. 13. Proposed subunit arrangement in the MAC (seen in frontal view as in Fig. 11, panel 5).

C6 and C7 have direct contact with C9 has not been analyzed as yet. Contact between C6 and C7 is implied from the observation of disulfide-linked C6, C7 heterodimers in the MAC [16]. The proposed subunit arrangement is consistent with photolabeling experiments using membrane-restricted probes and with the accessibility of subunits in the MAC to hydrophilic surface-labeling agents [19–21].

Heterogeneity of the MAC

The outcome of C5b-8-mediated C9 polymerization depends on the microenvironment of C5b-8's localization and on the supply of C9. Ideal conditions for tubular C9 polymerization by C5b-8 and for formation of the tubular MAC structure described in the previous paragraph are provided when single C5b-8 complexes are attached to single bilayer vesicles and an unlimited supply of C9 is present. Under these conditions virtually all C9 reacting with the complex is incorporated into an SDS-resistant MAC tubule and the final C5b-8:C9 ratio is 1:10–16 [10,22]. These findings are in agreement with the following argument. As mentioned above, 75% of tubular poly C9 consists of 14–16 C9 protomers; the remaining 25% extend the range of C9 protomers from 11 to 20 per tubule. The diameter of the poly C9 tubule is identical to that of the MAC-poly tubule. However, since our recent analysis of the composition of the MAC-poly C9 tubule indicates that it contains in addition to poly C9 one chain each of C6, C7, and C8, it would seem likely that the MAC-poly C9 tubule must contain fewer C9 molecules than a poly C9 tubule with an identical diameter. Assuming that the C6, C7, and C8 subunits require the same space as a C9

subunit (since they have a similar molecular mass), it may be argued that the MAC-poly C9 tubule contains three or four molecules of C9 less than poly C9. Based on these assumptions, the expected C5b-8:C9 ratio of the MAC is 1:10–12 for 75% of the complexes, which is in excellent agreement with measured ratios [10,22] under appropriate, ie, ideal, conditions. It should be remembered, however, that ideal conditions for C9 polymerization under normal conditions rarely exists. Two factors that probably restrict C9 polymerization and thus decrease the number of C9 molecules per C5b-8 is the tendency of C5b-8 to form clusters and the fact that natural membranes contain membrane proteins that may interfere with C9 polymerization. Clustering of C5b-7 and C5b-8 is enhanced when the complexes are assembled as intermediates in the absence of C9 or C8 and C9. If C5b-8 is bound in clusters, as recently directly demonstrated by Cheng et al [24], tubular C9 polymerization is restricted, and only about 20% or less of bound C9 is in the tubular, SDS-resistant form. If, in addition, the C9 supply is restricted, the proportion of SDS-resistant poly C9 is even lower than that. Under these conditions the observed C5b-8:C9 ratio varies from 1:6–8 to 1:1–3, depending on the supply of C9 [10,32]. The reason for the limited uptake of C9 by clustered C5b-8 even in the presence of an unlimited C9 supply may be twofold: (1) Owing to the density of C5b-8 complexes per unit surface area and owing to the possible presence of other membrane proteins, C9 access may be sterically restricted. (2) The probability is high at high C5b-8 density that polymerizing C9 makes contact with a second C5b-8 complex, resulting in the formation of complexes containing two or more C5b-8 complexes "cross-linked" by C9 oligomers (Fig. 14, left panel, arrows and arrowheads; virtually all lesions are interconnected in this micrograph). The latter reaction results in the formation of dimeric and oligomeric complexes [22] of very high molecular weight with relatively low C5b-8:C9 ratios. These complexes lack SDS-resistant poly C9 even though on membranes they form structures like membrane lesions owing to the curvature of polymerized C9 (Fig. 14, left panel). In Figure 14, (right panel), electron micrographs of extracted and purified complexes from cells with high MAC density (as shown in Figure 14, left panel) are depicted. It is evident that the majority of complexes consist of oligomeric structures (arrowheads) in which C5b-8 complexes seem to be cross-linked by noncircular C9 oligomers. In these complexes the average C5b-8 to C9 ratio is only 1:4–8 [22].

The interpretation given in the previous paragraph for the observed heterogeneity of the structure of the MAC owing to the various degrees of C9 polymerization is supported by a large body of data; however, it still remains, in part, controversial. Table III summarizes the main data published on C9:C8 ratios in the MAC over the last 13 years. In the following section, a discussion of some of the various observations is given, which, in our belief, reconciles most of the data with the interpretations above.

Structure of the MAC and SC5b-9 and the Dimer Hypothesis. The hypothesis that the MAC may be a C5b-8 dimer was originally proposed by us, based on the observation of Biesecker et al [35], that the S-rate and the molecular weight of the MAC was about twice that of the SC5b-9 complex after substracting the contribution of S-protein, which is not a component of the MAC. It was found that the structure of SC5b-9 and the MAC were very different and that SC5b-9 did not contain a tubule. This data contrasted with that of Bhakdi's group, who had reported that both complexes are monomeric, that their molecular weights were similar or identical, and that

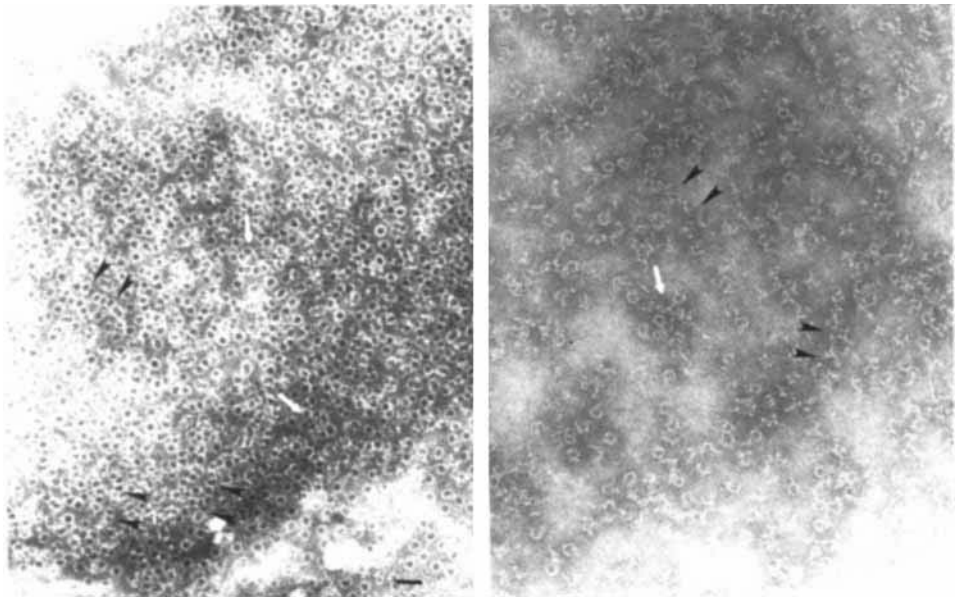

Fig. 14. Left panel) Ultrastructure of complement lesions formed on rabbit erythrocytes in undiluted human serum. Note the fusion of lesions to oligomeric interconnected complexes (black and white arrows) that consist of C5b-8 complexes cross-linked by oligo C9 (see text). Right panel) Ultrastructure of fluid phase oligomeric C5b-9 complexes extracted from membranes shown in the left panel and purified by gel-filtration of sepharose CL4B. Note the presence of large numbers of extended complexes lacking complete tubules (arrowheads) representing C5b-8 complexes cross-linked by oligo C9. Scale bar: 300 Å; staining: uranyl formate.

their ultrastructures were the same [36,37] except that the tubule of SC5b-9 was masked by S-protein. In retrospect, it is clear that Bhakdi's concept of a similar structure and mass of SC5b-9 and the MAC is no longer tenable because it was shown that S-protein blocks C9 polymerization and that SC5b-9 lacks the poly C9 tubule [45]. Thus, the main difference between the tubular MAC and SC5b-9 is as follows. C5b-8 induces circular C9 polymerization of 10–16 C9 molecules, thus creating the MAC-poly C9 tubule with its characteristic ultrastructural appearance [10,22]. When S-protein binds to C5b-8, only 2–3 C9 molecules are bound and a tubule is not formed [65]. The inhibition of C9 polymerization by S-protein thus explains both the ultrastructural difference and the difference in the mass of SC5b-9 and the MAC [65].

The polymerization of C9 by C5b-8 leads to the formation of a variety of C5b-9 oligomers as discussed above in which the C5b-9 dimer [23,25] is only one of the possible forms. It is likely that monomeric and dimeric complexes are in the minority on natural membranes under physiological conditions compared to higher oligomers. It thus becomes meaningless to discuss the monomer or dimer concept of the MAC [38].

The influence of the local environment on C5b-8-to-C9 interaction under otherwise identical conditions has been directly demonstrated by Tschopp et al [22] as follows. 1) Incubation of C5b-6, C7, C8 with a 12-fold molar excess of C9 and 15-fold molar excess of single bilayer vesicles results in the formation of tubular MAC-

poly C9 containing 10–14 C9 per C5b-8. If the molar excess of vesicles is reduced, resulting in the binding of more than one C5b-8 per vesicle under otherwise identical conditions, then the formation of tubular MAC-poly C9 is drastically decreased. A further reduction of MAC-poly C9 is observed when the complexes are assembled in fluid phase [22,31]. These experiments demonstrate that clustering of C5b-8 directly affects circular C9 polymerization as measured by resistance to dissociation by SDS and C9 uptake. 2) That clustered C5b-9 complexes have a high molecular weight and fewer C9 molecules per C5b-8 owing to cross-linking of C5b-8 by oligo-C9 is supported by the finding that MAC complexes extracted from rabbit erythrocytes and fractionated by gel-filtration show the following C5b-8 to C9 ratios. Fractions eluting with an apparent molecular weight of $3–5 \times 10^6$ (and higher) contain a C5b-8 to C9 ratio of 1:3–4 and no tubular MAC-poly C9, whereas fractions eluting with an Mr of approximately 1.5×10^6 show average C5b-8 to C9 ratios of 1:6 and do contain tubular MAC-poly C9 [22] (see also Fig. 14).

Taken together, these experiments clearly support the concept that the multiplicity of the C5b-8 complex and the consequent clustering have a strong effect on MAC assembly and determine whether tubular MAC-poly C9 or oligomeric structures are formed. Further support for the hypothesis that C9 binding and polymerization by C5b-8 depends on the microenvironment comes from experiments by Rauterberg et al [39], who demonstrated by immunoelectronmicroscopy that only a fraction of membrane-bound C9 antigens is associated with membrane lesions. This finding can be interpreted to indicate that many C5b-8 complexes are unproductive in the formation of ultrastructural lesions because tubular C9 polymerization is inhibited by local conditions.

The C5b-8 to C9 Ratio. There is now general agreement that several C9 molecules bind per C5b-8 complex (see Table III). Our own determinations indicated [10] that under conditions of serum excess and *nonstepwise* assembly of the MAC the average C5b-8 to C9 ratio on the rabbit erythrocytes is 1:5–8. This value is consistent with earlier studies by Kolb et al [27] and was confirmed by Bhakdi et al [36], who reported values of 1:6–8 for both sheep and rabbit erythrocytes. We also found under special conditions that the C5b-8 to C9 ratio can be 1:10–12 (−16) provided that the C5b-8 is not clustered *and* the MAC is assembled in a *nonstepwise* manner [10]. It was pointed out in the discussion in the previous paragraph that local conditions can strongly interfere with tubular C9 polymerization leading to decreased C9 uptake. Thus, if the aim is to determine the maximal possible uptake of C9 by C5b-8, precautions have to be taken against C5b-8 clustering to itself or to membrane proteins. Stewart et al [33], for instance, found, under no conditions, an uptake of C9 exceeding a 1:3–4 ratio. These authors assembled the MAC in a stepwise fashion either after preparing first EAC1-7 or EAC1-8 and then adding C8 and C9 simultaneously or C9 alone. As mentioned in one of our earlier studies [10], the stepwise assembly of the MAC from EAC1-7 or ECA1-8 results in C5b-8 to C9 ratios of 1:3.8 (exactly as confirmed by Stewart), and it was pointed out that for accurate determinations of C5b-8:C9 ratios it is necessary to assemble the complex in a *nonstepwise* manner simulating in vivo conditions. Complement lesions assembled on erythrocytes by a stepwise assembly as done by Stewart et al [33] in fact are quite irregular and condensed compared to normal lesions (Fig. 15). The left panel (Fig. 15) shows EC5b-8 (arrow pointing to clustered C5b-8 on the membrane edge). If these EC5b-8, after washing, are incubated with excess C9, the image in the right panel (Fig. 15) is

TABLE III. Molecular Ratios of C5b-8 to C9 in C5b-9 Complexes*

Method of determination	Type of membrane	No. of C5b-8 per particle	Probably predominant state of C5b-8	Stepwise assembly of C5b-9	C8:C9 ratio[a]	Electron microscopy	Reference
A. *Functional Studies (pore size)*							
Hemolysis	Es	ND	ND	Yes	1:1[f]	ND	26
Hemolysis	Es	100	Clustered	Yes	1:3[f]	ND	27
Release of sucrose	Eh	200–1500	Single?[b]	Yes	1:3[f]	ND	28
Release of inulin (30 Å diameter)	Es	ND	Single?[b]	Yes	1:2–3[f]	ND	
Release of RNAse (38 Å diameter)	Es	ND	Single?[b]	Yes	1:4–5[f]	ND	29
Release of ovalbumin and hemoglobin (>55Å–<150Å)	Es	ND	Clustered	No	ND[g]	ND	30,51
B. Binding and extraction studies							
Binding of radiolabeled proteins	Es	20–200	Clustered	Yes	1:6	ND	27
Hemolytic *consumption*	Fluid phase	NA	Clustered	Yes	1:2.9	ND	31
Binding competition	Er	25,000	Clustered	No	1:5–8	Lesions above 1:3 ratio[a]	10

Method of determination	Type of membrane	No. of C5b-8 per particle	Probably predominant state of C5b-8	Stepwise assembly of C5b-9	C8:C9 ratio[a]	Electron microscopy	Reference
Binding	Er	3700	Single	No	1:10–12(15)	Lesions	10
Antigen consumption	Er, Es	High	Clustered	No	1:6–8	Lesions above 1:3 ratio[a]	32
Binding of radiolabeled proteins	Es	50–4,000	Single?[b] Clustered	Yes	1:3–4	ND	33
Binding and SDS-PAGE	Lecithin vesicles	ND	ND	Yes	Average 1:6[c] up to $C9_{12}$	ND	5
Binding and SDS-PAGE	Lecithin vesicles	1	Single	No	1:10–12[d]	ND	22
Binding and SDS-PAGE	Lecithin vesicles	ND	ND	No	1:10–16[e]	ND	16

*ND, not determined.

[a]Irregular lesions at 1:3 ratio; normal lesions at 1:6.

[b]Even though the total number of complexes per cell is low, it is not certain whether the majority is single or clustered.

[c]Measured as disulfied-linked C9 oligomers by SDS-PAGE.

[d]Measured as SDS-resistant MAC-poly C9.

[e]Measured by densitometry after dissociation of MAC-poly C9 with guanidine-isothiocyanate.

[f]Measured ratio was required for the functional effect under analysis and may not represent maximum possible binding.

[g]No C5b-8:C9 ratios were measured; these results are shown as examples that functional pore sizes of ~ 100 Å can be achieved.

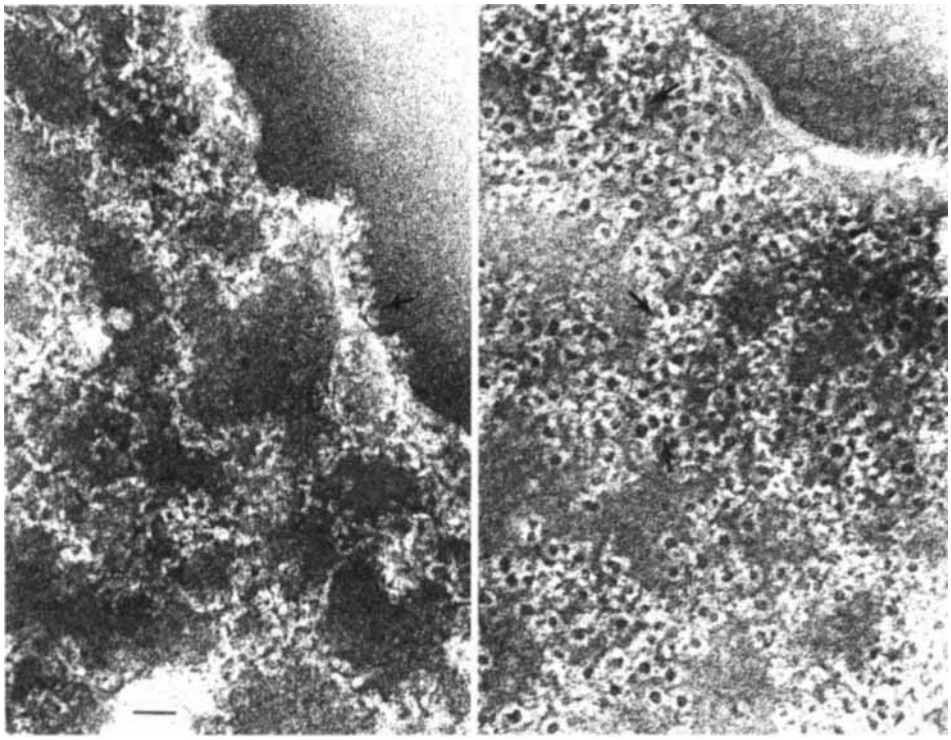

Fig. 15. Left panel) Ultrastructure of C5b-8 complexes on rabbit erythrocytes incubated with C9-depleted serum. Note the aggregated, often linear, arrays of clustered C5b-8 complexes. The arrow points to complexes seen on the membrane edge. Right panel) Condensed appearance of membrane lesions generated from EC5b-8 (left panel) by stepwise assembly. Note the irregular appearance of lesions compared to those of Figure 14 (arrows). C5b-8:C9 ratio was 1:3.8. Scale bar: 250 Å.

obtained. Comparison of these lesions (assembled stepwise) to lesions assembled nonstepwise (Fig. 14, left panel) reveals the striking structural difference corresponding to decreased C9 uptake: C5b-8:C9 = 1:3.8 for stepwise assembly versus 1:5–8 for nonstepwise assembly. The conditions for uptake used by Stewart et al [33] thus favor the low C9 uptake, presumably owing to C5b-8 clustering or association with membrane proteins even at low C5b-8 density. In addition, it is necessary to determine whether the purified C9 is active by determining its incorporation into macromolecular complexes [10]. If a large proportion of C9 is not bound [33] to the MAC or SC5b-9, erroneous uptake results may be obtained.

Direct evidence for the formation of C9 polymers with 7 to 12 protomers ($C9_7$–$C9_{12}$) in the MAC was provided by Yamamoto et al on SDS gels subsequent to disulfide cross-linking of C9 monomers [15]. These studies demonstrated the presence of up to 12 C9 monomers in the MAC directly linked to each other and lend final support to the concept that at least 12 C9 molecules can be bound per C5b-8 (Table III).

In functional studies (Table III), it has been shown that the release of larger markers from resealed ghosts requires a higher multiplicity of C9 per C5b-8. However, it has not yet been determined how many C9 molecules in the MAC are required

to produce a 100 Å functional lesion. From studies by Ramm et al [29], it is clear that more than 4–5 C9 per C5b-8 are necessary for lesions exceeding a functional diameter of 40 Å. Functional studies with erythrocytes are complicated by an additional element first pointed out by Bauer et al [40] and recently also observed by Sims [28]. Shape change of red cells and marker release is dependent on a critical number of complexes per cell (750 or 300 C5b-9 per cell, respectively). How this effect relates to C9 polymerization and to C5b-8 to C9 ratios is not clear at the present time.

The reactions discussed may be summarized as in Table IV. The heterogeneity of the structure of the membrane attack complex owing to the formation of C9 polymers with subunit numbers from 1 to 16 and owing to the formation of oligo-C9 cross-linked C5b-8 complexes, is probably responsible for the observed heterogeneity of functional pore sizes [49–54]. It may be predicted with a high degree of probability that the tubular MAC forms functional membrane pores of a size closely correlated to its ultrastructure similar to the findings with homogeneous tubular poly C9 [9,41].

Functional Effects of the MAC on Target Membranes. It is evident from numerous recent studies that one of the cytolytic effects of the MAC is mediated by the formation of a stable transmembrane pore [9,30,51] that dissipates ionic gradients maintained by the membrane and allows the egress of macromolecules from attacked cells and the entry of Ca ions and other molecules such as lysozyme. These events lead to a breakdown of the membrane potential and to rapid loss and depletion of intracellular ATP pools, which probably contributes to cell death. In bacterial targets the entry of lysozyme results in the destruction of the peptidoglycan skeleton, the loss of gross morphology, and accelerated cell death [47].

More controversial has been our proposal that in addition to channel formation the MAC physically disrupts the membrane integrity owing to its lipid binding capacity and its space requirements upon insertion and polymerization of C9 [42–44]. For instance, Bhakdi has repeatedly argued that MAC insertion into membranes results in pore formation but that otherwise the membrane integrity remains intact and results in stable MAC-lipid association [34,38,45]. This interpretation was based on the recombination of already assembled complexes by the detergent dialysis technique with phospholipid bilayers. This technique, in essence, assembles bilayers around preformed complexes, whereas under normal conditions the complex assembles in a preformed membrane. This distinction is important with regard to the physical membrane disruption for the following reasons: (1) Upon membrane insertion of C5b-8 and subsequent C9 polymerization, a complex of ~110 Å diameter is assembled *in the membrane* that occupies an area of about 10,000 $Å^2$. Lipid or protein molecules previously located in this area are either laterally displaced or expelled from the membrane. It is easy to see that a gross alteration of the physical integrity of the membrane must occur when 30,000 to 200,000 such complexes are inserted into a cell (see, eg, Fig. 14) simply by the lateral displacement of membrane

TABLE IV. Heterogeneity of the MAC Owing to Variable Surface Density of C5b-8

State of C5b-8	No. of C9/C5b-8	Structural formula	SDS-resistant tubule	Molecular weight
Single	10–16	$C5b\text{-}8,C9_{16}$	Yes	1.7×10^6
Clustered	~6	[a]$(C5b\text{-}8)_{2\text{-}5}\ C9_{5\text{-}30}$	No	$2\text{-}4 \times 10^6$

[a]Putative range occurring under physiological conditions on natural membranes.

components by MAC-poly C9 and the resulting membrane surface expansion. In the case of single bilayer phospholipid vesicles, a high multiplicity of complexes per vesicle causes a disassembly of the bilayer [46]; similarly, the disassembly of viral membranes by this mechanism was reported by Esser et al [42]. In the case of bacteria attacked by the MAC in the absence of lysozyme, an approximately twofold expansion of the outer membrane was observed [47] owing to the insertion of large numbers of membrane attack complexes. These changes are independent of channel formation in as much as a similar expansion would be effected by the insertion of solid plugs of 100 Å diameter. The presence of a pore structure in MAC-poly C9, of course, facilitates lysis of those membranes that act as barriers of ionic gradients. In addition, the pore structure allows the entry of lysozyme through bacterial outer walls, resulting in the breakdown of the peptidoglycan layer. (2) As discussed above, C5b-8-mediated C9 polymerization on natural membranes gives rise to a large proportion of nontubular poly C9. Insertion of a half-tubule into a membrane leads to an unstable condition of the lipid bilayer because the luminal face of the tubule, the concave inner surface of C9 protomers, in all probability is hydrophilic and repels the hydrophobic chains of phospholipid molecules. It is likely that under these conditions the permeability increase is mediated partly by a protein pore and partly by lipid rearrangements. In this context, the observation by Esser's group [48] that thrombin-cleaved C9, which forms only linear membrane-inserted polymers, is hemolytically as active as intact C9-forming tubular polymers is not surprising. The conclusion by this group that tubular C9 polymerization is merely coincidental, however, ignores the fact that tubular polymerization greatly stabilizes poly C9 against degradation by proteases and dissociation by detergents even in the absence of covalent disulfide exchange.

In summary, it appears that assembly of the MAC and polymerization of C9 facilitates two modes of membrane attack by complement. Clustering of C5b-8 by the focal activation of C5 molecules promotes the assembly of C5b-9 clusters in which both circular (tubular) and noncircular MAC-poly C9 complexes in various oligomeric states are found. This assemblage gives rise to both the formation of stable pores and causes physical disruption of the bilayer. Depending on the type of membrane either one or both mechanisms may be responsible for the ultimate cytolytic effect of the MAC.

The Insertional Reaction: Formation of the C5b-7 Complex

The reaction sequence of C5b-7 insertion and MAC assembly is summarized in Figure 16, including the control reaction of S-protein discussed below. No further proteolytic cleavage takes place after activation of C5, indicating that expression of hydrophobicity by C5b-7, C5b-8, and MAC must be mediated by other mechanisms. As discussed above, expression of hydrophobic domains in the lytic reactions is caused by unfolding of the C9 molecule following high-affinity C9-C9 interaction. It appears that the expression of hydrophobic domains in the insertional step also is caused by unfolding of interacting subunits of the C5b-7 complex, resulting in the formation of a hydrophobic membrane combining site. The main component in the insertional reaction is C7. However, unlike C9, the insertional reaction mediated by C7 does not set into motion a polymerization reaction and thus does not assemble a tubular lytic complex.

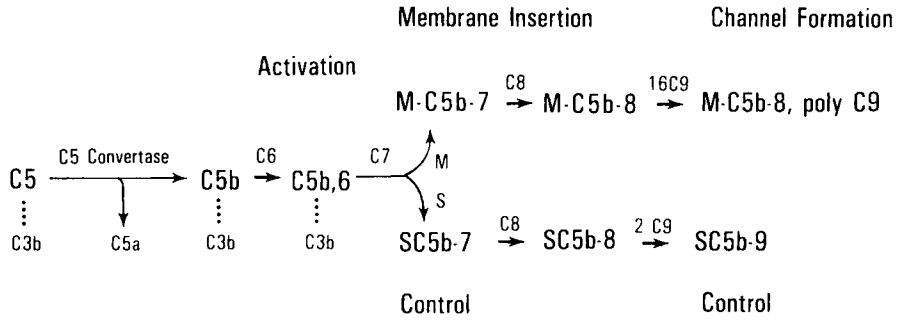

Fig. 16. Schematic sequence of the MAC assembly and control after activation of C5. M, membrane; S, S-protein of plasma.

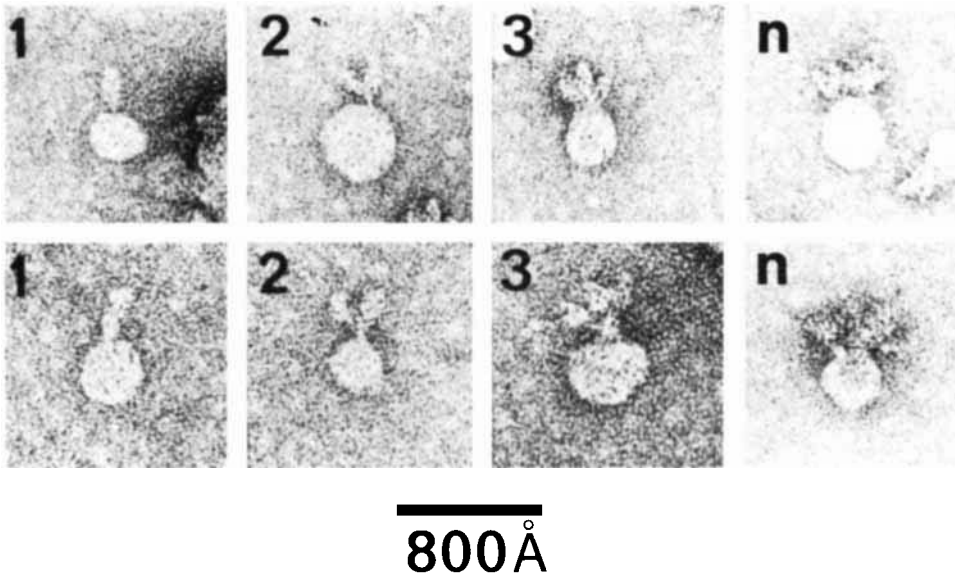

Fig. 17. Structure of C5b-7 complexes bound to single bilayer vesicles. Monomeric (1), dimeric (2), trimeric (3), and oligomeric (n) C5b-7 complexes are shown in association with phospholipid vesicles.

Structure of C5b-7

Reaction of C7 with C5b-6 in stoichiometric amounts results in the formation of an amphiphilic complex containing a narrow membrane combining site [55,56]. If complex formation occurs on the surface of lipid bilayer membranes, the hydrophobic combining site inserts itself into the bilayer and anchors the C5b-7 complex (Fig. 17) in the hydrocarbon core. Membrane-bound C5b-7 appears as a ~280 Å long rod structure projecting above the membrane surface; the length of the inserted membrane binding site is between 20 Å and 40 Å. Membrane-bound C5b-7 complexes have a strong tendency to form clusters. In figure 16, monomeric (1), dimeric (2), trimeric (3), and oligomeric (n) complexes are shown. Oligomeric complexes appear to cause

permeability increases as suggested from the penetration of negative stain into the single bilayer vesicles bearing three or more complexes. The clustering of C5b-7 in the membrane is mediated by the hydrophobic domain and indicates high-affinity protein-protein interaction even in a hydrophobic environment. Based on the less pronounced tendency to clustering of C5b-8 [55], it may be speculated that part of this clustering site contains a binding site for one of the C8 subunits.

If C5b-7 is generated in fluid phase, the forming C5b-7 complexes aggregate by interaction of their hydrophobic domains and form soluble protein micells of snowflakelike appearance in the electron microscope [55]. Since this aggregation is not reversible in detergents such as deoxycholate, it is likely that the high-affinity protein-protein interactions discussed for the membrane-bound C5b-7 are responsible for the detergent-resistant association of C5b-7 complexes.

The membrane combining site of C5b-7 is made up, in part, by C7 as determined with biotinyl C7 and kolloidal gold coated with avidin, whereas the C5b-6 unit is distal to the hydrophobic domain as determined by the same technique. Since the biotin labeling technique labels mainly C5b in C5b-6, this result is interpreted to mean that C5b is located on the end of C5b-7 opposite to its membrane combining site [57,58].

Conformational Rearrangement During C5b-7 Formation

Interaction of the two hydrophilic precursors, C5b-6 and C7, gives rise to an amphiphilic complex. The hydrophilic-amphiphilic transition is accompanied by an increase in β-structure of the complex, by an increased acidity, and by the expression of neoantigens. Together with the increased length of C5b-7, these changes may be interpreted as a restricted unfolding of subunits of C5b-7 (Fig. 18). One of the subunits capable of undergoing such a change is C7 (see below). Whether C5b or C6 are also involved in the restricted unfolding remains speculative. The formation of disulfide-linked C6-C7 dimers during MAC assembly and the composition of MAC-poly C9 (see above) may argue for a participation of C6 as well.

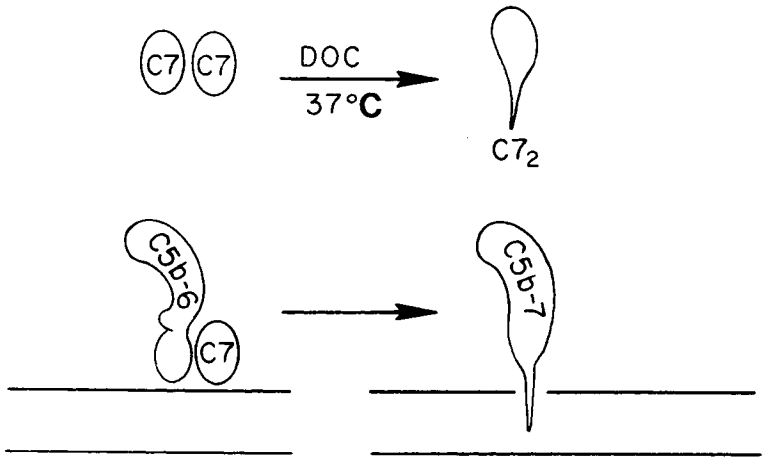

Fig. 18. Hypothetical scheme for the generation of hydrophobic domains in C5b-7 and in C7 dimers.

Formation of Amphiphilic C7 Dimers

Incubation of C7 with sodium deoxycholate at 37°C results in the formation of 7.3S C7 dimers with amphiphilic properties [57]. C7 dimers recombine with phospholipid vesicles in the detergent dialysis procedure. In the absence of detergents, C7 dimers aggregate owing to their hydrophobic combining sites.

Incubation of C7 at 37°C with 1 M guanidine HCl results in the formation of linear C7 polymers that remain hydrophilic. This polymerization reaction in guanidine appears to be analogous to the one observed with C9 under similar conditions. C5 and C6 do not show the properties of dimerization and polymerization of C7 and C9, respectively.

The transition of C7 during dimerization may be considered as a model reaction for the hydrophilic-amphiphilic transition of C5b-6 upon reaction with C7 (Fig. 18). The likely reaction partner of C7 in the trimolecular complex is C6 as suggested from its similar structure and its incorporation into C6-C7 dimers and into the MAC-poly C9 tubule along with C7 and C8α-γ.

The C5b-8 Complex

C5b-7 serves as acceptor for C8 in stoichiometric amounts. In contrast to C5b-7, C5b-8 mediates low levels of cytolytic activity [53,59]. It is probable that dimeric or oligomeric C5b-8 complexes are required for cytolysis to occur. C5b-8 does not cause the formation of ultrastructural lesions. The pore size of C5b-8-mediated functional lesions is rather small (8–12 Å) compared to that of the MAC (C5b-8, poly C9) (up to 70–110 Å). C5b-8 retains the rod structure of C5b-7. The C8 molecule appears to be located in the center of C5b-7 close to the membrane surface in the inserted complex (Fig. 19). The fact that C5b-8 mediates cytolytic activity may be interpreted to indicate that the previously completely hydrophobic domain of C5b-7

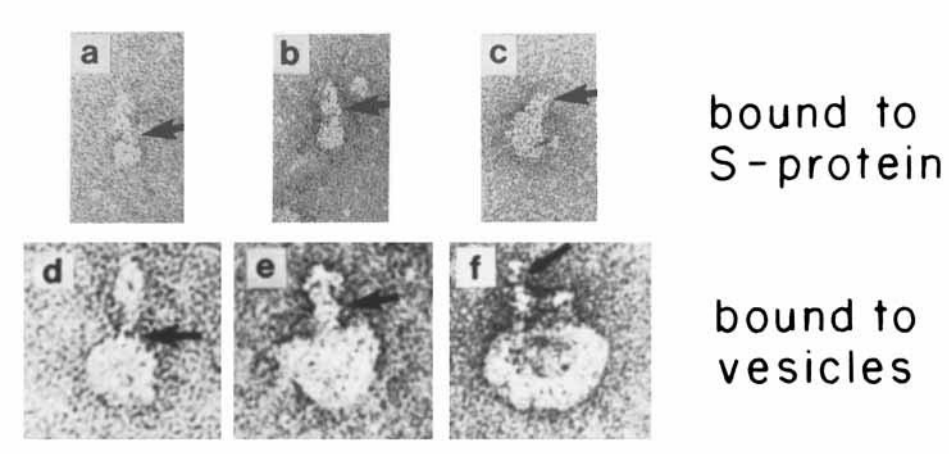

Fig. 19. Structural assembly of SC5b-9 bound to S-protein (a–c) and of the MAC on single bilayer phospholipid vesicles (d–f). a) SC5b-7. b) SC5b-8. c) SC5b-9. d) Vesicle C5b-7. e) Vesicle C5b-8. f) Vesicle MAC = [C5b-8 (poly C9)]. The arrows point to the narrow hydrophobic combining site of C5b-7 inserted in the membrane or covered by S-protein (a,d), to the site of C8 in C5b-8 (b,e), and to the C5b containing region in SC5b-9 and MAC (c,f).

has acquired a hydrophilic face upon binding of C8. This hydrophilic face of the membrane-inserted complexes may subsequently be enlarged by binding and polymerization of C9 to form the hydrophilic tubule lumen.

Control of Membrane Attack by Complement

Control occurs at both stages of MAC assembly, the insertional step, and the step of C9 polymerization.

Inhibition of C5b-7 Insertion

Release of C5b-6 or C5b-7 complexes from activating particles can cause lysis of bystanding cells (reactive lysis) by insertion of C5b-7 and binding of C8 and C9 [60,61]. Reactive lysis is inhibited by plasma lipoproteins, C8, and S-protein [62–64]. The inhibitory action of each of these C5b-7 inhibitors is caused by physical association of the inhibitor with the complex, rendering the forming complex incapable of inserting into membranes. Lipoproteins presumably bind to C5b-7 by virtue of their content of lipids, which may resemble a membranelike environment for C5b-7 insertion. C8 binding to C5b-7 is specific and leaves the forming C5b-8 complex amphiphilic. The failure of C5b-8 to insert into membranes may be due to an alteration of the hydrophobic combining site. It is possible that this site, after binding of C8, becomes too bulky or that it expresses now a hydrophilic face (see above) on that side that is destined to face the tubule lumen after binding and polymerization of C9. Both lipoproteins and C8 do not interfere with subsequent binding of C9. S-protein binds to the membrane binding site of C5b-7 and renders the forming SC5b-7 complex water soluble (Fig. 19a–c). We encounter here the unique sequence that two hydrophilic proteins, C5b-6 and C7, undergo a hydrophilic-amphiphilic transition and form the amphiphilic C5b-7 complex, which, after association with another hydrophilic protein, the S-protein, undergoes an amphiphilic-hydrophilic transition to the hydrophilic SC5b-7 complex.

The structure of SC5b-7 is a ~340 Å long rod in which S-protein is bound to the membrane binding site of C5b-7 opposite to the site of C5b (Fig. 19a). Binding of C8 and C9 does not appreciably change the ultrastructure of the complex (Fig. 19b,c).

Inhibition of C9 Polymerization

S-protein associated with C5b-8 blocks circular (tubular) C9 polymerization even though 2–3 C9 molecules are associated with the SC5b-9 complex [65]. The mechanism by which S-protein interferes with C9 polymerization is not known. Figure 20 compares the ultrastructure of the MAC and the SC5b-9 complex. The lack of the tubular poly C9 structure in SC5b-9 correlates with the lack of a high molecular weight poly C9 band on SDS-polyacrylamide gels of SC5b-9.

Initial evidence is accumulating that C9 polymerization by C5b-8 on membranes or C9 insertion may be under the control of lipoproteins (HDL) and membrane proteins of host cells [66,67]. The observation of sequence homology in C9 and LDL receptors may be of significance for the inhibitory action of lipoproteins.

ASSEMBLY OF CYTOLYTIC COMPLEXES BY CTL AND NK LYMPHOCYTES

Introduction

The molecular mechanism of lymphocyte-mediated cytolysis has long been enigmatic. As recently as 1983, a volume of Immunological Reviews ("Mechanism

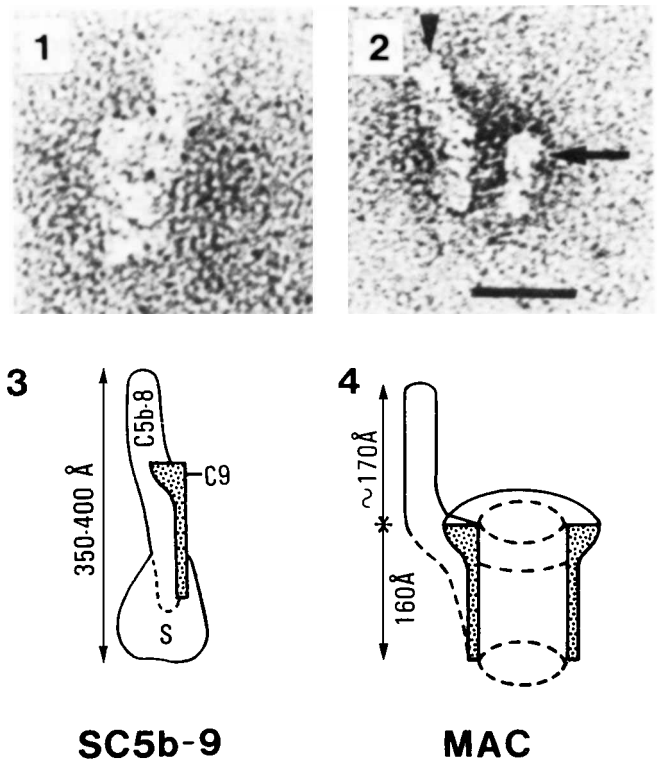

Fig. 20. Structural comparison of SC5b-9 (panel 1,3) and the MAC (panel 2,4) demonstrating the lack of poly C9 in the SC5b-9 complex. Panels 1 and 3 are rotated by 180° with respect to each other. The arrowhead in 2 depicts the location of C5b; the arrow points to the poly C9 torus. Scale bar: 200 Å.

of Action of Cytotoxic cells"), containing articles by Berke [68], Brooks et al [69], Martz et al [70], Russell [71], and Bonavida et al [72], demonstrated the various views of workers in this field.

With the discovery of cytolytic granules (by this laboratory [73,82] and by Henkart's [74] group) present in NK cells and in CTL, it is now possible to propose a molecular mechanism for lymphocyte-mediated cytolysis that can explain both the "kolloid osmotic" and the "internal disintegration" [71] or "zeiosis" [75] or "apoptosis" [76] model of CTL lysis. The difference between these two types of lysis is the supposition that in the kolloid osmotic lysis the target cell's plasma membrane is damaged in a manner similar to the effects of complement on targets. In contrast, zeiosis or apoptosis is believed to affect first and mainly the target nucleus and has been described as lysis originating internally.

Isolated granules from CTL contain mediators responsible for both kolloid osmotic lysis as well as for nuclear disintegration and apoptosis. As will be discussed in the end of this chapter, granule-mediated cytolysis thus can explain in molecular terms the two seemingly contradictory models described above.

The Pore Forming Activity of Granules

The first evidence for the formation of membrane lesions in lymphocyte-mediated cytolysis came from studies using human peripheral blood lymphocytes as

effector cells for antibody-mediated erythrocyte lysis [77]. Subsequent work with cloned murine NK cells and CTL as well as with a rat NK-like tumor cell line confirmed and extended this initial observation [73,78,79]. Figure 1 shows the ultrastructure of membrane lesions induced on target cells by cloned NK or CTL in comparison to human complement lesions. The observation of these lesions suggested that they too arise by polymerization of monomeric precursor proteins and that they form transmembrane channels similar to poly C9 of complement. These lesions were therefore named poly perforin 1 (160 Å diameter) and poly perforin 2 (~70 Å diameter). Subsequent work to be outlined below confirmed this original hypothesis and led to the characterization of T-cell perforin 1 as the first cytolytic protein isolated from cytolytic T-lymphocytes [80].

Cytolytic Granules From NK-Like Cells and CTL Contain the Perforins

Morphological studies had indicated that the monomeric precursors (perforins) giving rise to tubular poly perforins were located in the cytoplasmic granules of cloned killer lymphocytes [50–52, 73,74,78,79,81]. Isolation of granules by Percoll density gradient centrifugation and their analysis showed that isolated T-cell granules are highly cytolytic for erythrocytes and for tumor targets. Cytolysis is absolutely Ca dependent and strongly temperature dependent. At 37°C lysis of target cells by purified granules is complete within 2–5 min. The cytolytic event is accompanied by the assembly on membranes of poly perforin 1 (poly P1) and poly perforin 2 (poly P2) [73,74]. Since granules incubated without Ca do not contain the tubular poly perforins, it became evident that transmembrane tubules, as previously suggested, assemble during the lytic reaction in a Ca-dependent step from granule-contained monomeric precursors.

Cytolytic granules have been isolated from a number of CTL and NK-like clones [for review, see 82]. Particularly from NK-like clones, it is easy to demonstrate Ca-dependent granule-mediated cytolysis in a hemolytic assay. Typical H2-restricted T-cell clones seem to have fewer granules per cell and a lower amount of hemolytic activity per unit weight of isolated granules. It is possible, therefore, that there are quantitative differences in the content of perforin 1 and 2 between different T-cell clones and NK cells.

Granule-mediated cytolysis lacks specificity (Fig. 21) and all tumor targets tested are efficiently lysed. The difference in susceptibility to granule-mediated lysis of various tumor cells may be attributable to repair mechanisms of the target cells or to different binding affinities of granules to tumor targets. The lack of specificity of granule-mediated lysis implies that specific killing by *intact* CTL is caused by specific recognition by the antigen receptor and other adherence molecules, whereas the cytolytic step *per se* is unspecific. This situation is analogous to complement where the cytolytic sequence also is unspecific and requires direction by the alternative or classical pathway of complement activation.

Antisera raised to isolated granules from CTLL2, an orginally H2-restricted, cytolytic T-cell that has lost cytotoxicity as intact cell but retained cytolytically active granules, recognize and bind to cytoplasmic granules of all cytolytic lymphocyte clones tested regardless of whether they show NK-like or MHC-restricted CTL specificity. This finding further emphasizes that the cytolytic machinery of various cytolytic clones with different specificity is identical and thus that granules are not clonotypic. Furthermore, it demonstrates that NK and CTL share the cytolytic

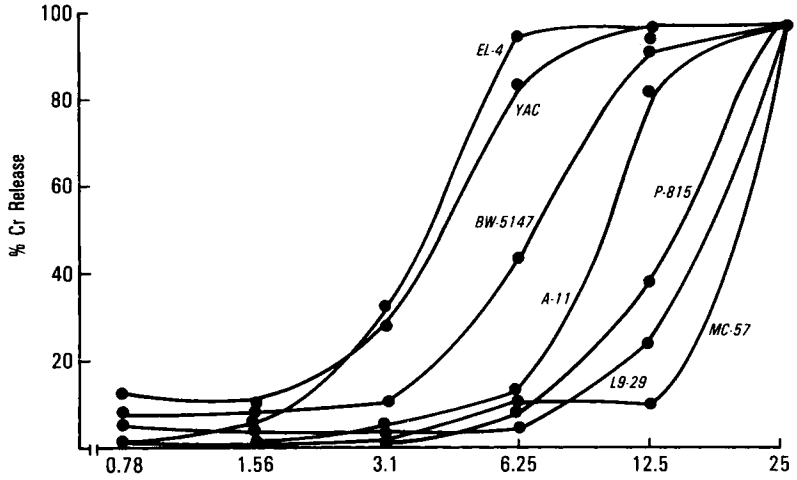

Fig. 21. Granule-mediated cytolysis of various tumor cells. Note the logarithmic scale of the abscissa.

mechanism. Granules from noncytolytic T-lymphocytes, T-lymphomas, or splenocytes are not recognized by anticytolytic-granule-specific antiserum, indicating that cytolytic granules of CTL and NK cells contain a distinct set of antigens not present in granules of other cells.

The role of granules in the cytolytic event mediated by intact CTL is evident from an immunofluorescent study shown in Figure 22. After conjugation with the target cell, the killer cell undergoes a polarization that brings the microtubule organizing center and the Golgi complex into the vicinity of the contact site [83,84]. As shown in Figure 22, this polarization reaction also moves the cytolytic granules to the contact area. The granules subsequently are released by directed secretion onto the target membrane. It is speculated that this reaction is responsible for target cell lysis by causing Ca-dependent perforin polymerization and transmembrane channel formation similar to that observed with isolated granules described (Fig. 23). Subsequently, factors enter the cell causing DNA degradation (see below).

Nuclear Disintegration by Granules

As reported by Russell et al [71,85], CTL cause the release of both, cytoplasmic and nuclear markers (DNA) from target cells. Nuclear DNA is released as 200 base pair fragments and multiples thereof, suggesting DNA cleavage between nucleosomes as a result of CTL killing [76]. Figure 24 shows that isolated cytolytic granules from the murine CTLL2 T-cell line cause release of ^{51}Cr and ^{3}H-thymidine from EL4 target cells [86]. The released DNA is fragmented to 200 bp and multiples. This observation suggests that the factor(s) responsible for T-cell-mediated target DNA degradation are also contained in isolated cytolytic T-cell granules.

Molecular Nature of the Nucleolytic Factor of Cytolytic Granules

The following observations may suggest that the factor of isolated granules responsible for DNA degradation may be similar to lymphotoxin (LT) or tumor necrosis factor (TNF): (1) Isolated CTL granules lyse L929 cells, the classical target

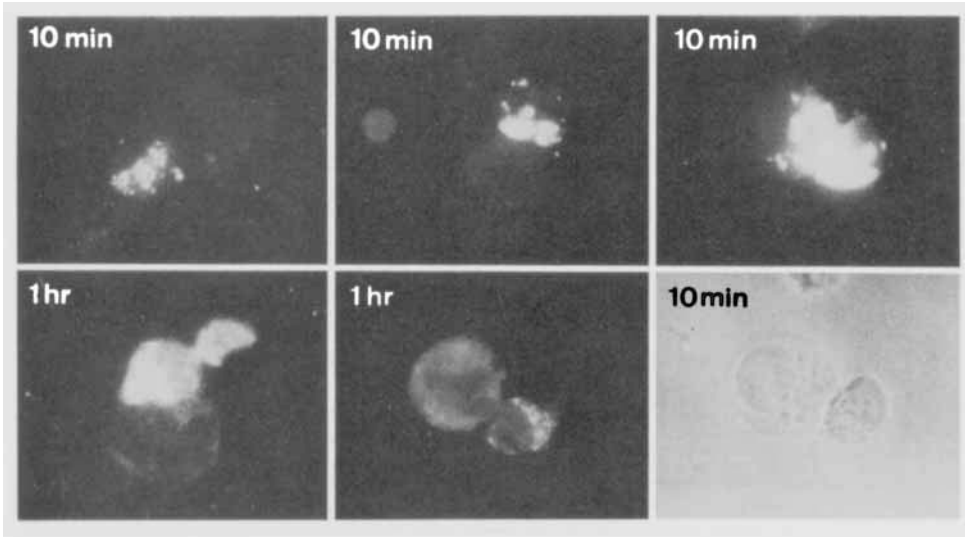

Fig. 22. Demonstration of the participation of cytoplasmic granules in T-cell-mediated cytolysis. Killer-target conjugates, after 10 min or 1 hr at 37°C were fixed, permeabilized, and stained with antigranule antibody and fluorescenated second antibody. The fluorescence of several conjugates is shown; the two panels on the right show the corresponding flurorescence and phase photo micrographs. Note that the granules in all conjugates are located close to the killer-target conjugation site and that target granules (although present) do not stain with the antiserum.

for LT or TNF, even when the perforin system has been inactivated by preincubation with Ca in the presence of serum. Granules thus contain an LT- or TNF-like activity that remains active in the presence of Ca ions and in the presence of serum. (2) Isolated CTL granules, even after inactivation of the pore forming perforin system by preincubation with Ca, cause target DNA degradation to the typical 200 bp ladder. Isolated perforin 1 does not cause DNA degradation during tumor cell lysis.

Taken together, these observations could suggest that granules conatin an LT- or TNF-like activity that is responsible for the observed DNA degradation. This indirect evidence supports findings by Ruddle's group [87] suggesting that LT causes DNA degradation.

Finally, the finding that LT and TNF, as well as NKCF (natural killer cytolytic factor) [88–90,93] released upon specific or nonspecific stimulation of cytolytic lymphocytes is consistent with their prior location in storage sites, possibly representing cytolytic granules. Whereas the released perforins are immediately inactivated upon release by Ca and serum proteins, the other factors (LT, TNF, NKCF) retain their activity.

Delivery of Nucleolytic Factor(s) to Target Cells

Whether the nucleolytic factor (NF) of CTL granules in fact is identical with LT, TNF, or NKCF, or represents an independent molecule has not been determined. That NF can be delivered from granules to the target nucleus via the pore forming system is implied from the different kinetics of DNA degradation in the presence or absence of active perforins. Intact granules containing active perforins and nucleolytic factor(s) lyse targets within 30 min at 37°C. In the same time span, DNA degradation

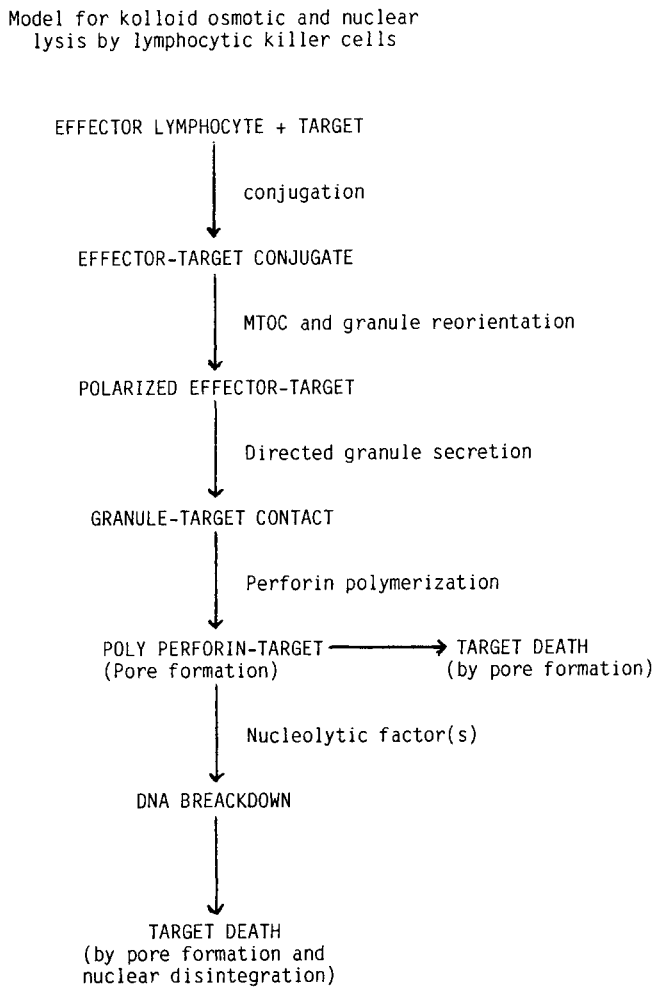

Fig. 23. Sequence of steps leading to granule-mediated cytolysis of target cells by pore formation and DNA degradation.

by granule NF is detectable. In contrast, when the perforin system of granules has been inactivated, several hours are required for DNA degradation to occur. This kinetic difference probably indicates that the rapidly formed poly perforin pores can be utilized for entry of NF, which in turn triggers DNA degradation. In the absence of the poly perforin complexes, NF uptake may be much slower and less quantitative through receptor-mediated or endocytotic mechanisms resulting in protracted DNA degradation and lysis.

Kolloid Osmotic Lysis and Apoptosis Caused by Cytolytic Granules

The previous discussion clearly shows that granules are endowed with several cytolytic factors that can act independently or in a synergistic fashion. The outcome as to whether in a given target kolloid osmotic lysis or nuclear disintegration predom-

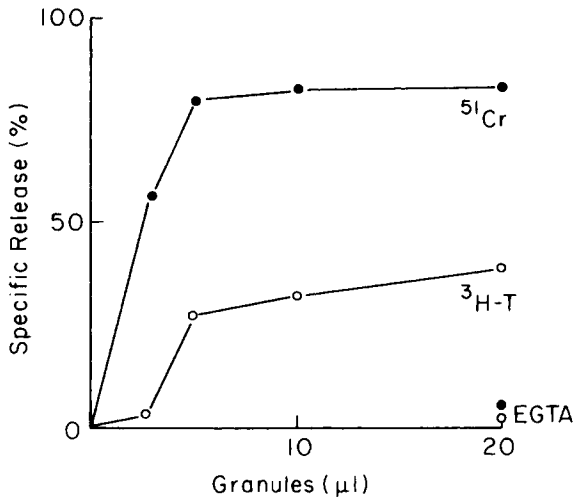

Fig. 24. Release of cytoplasmic (^{51}Cr) and nuclear (^{3}H-thymidine) markers from E1 4 targets lysed by isolated CTLL2 granules. The assay was carried out for 20 min at 37°C.

inates may depend on the nature of the target cell and on the quantity of granules delivered. For instance, it is possible that in CTL killing only a few (say 100–1,000) poly perforin complexes per target cell are formed and that the major damage is caused through the entry of NF through these channels. The appearance of apoptosis would predominate even though transmembrane pores were present and actually were essential for cell killing. If, on the other hand, a target cell is resistant to nucleolytic factors, kolloid osmotic lysis would predominate. Similarly, the outcome could be dependent on quantitative differences in the composition of granules from various clones containing different ratios of perforin and NF.

Composition of Cytolytic Granules and Characterization of Perforin 1

Granules isolated from CTLL2 have a relatively complex protein pattern as shown in Figure 25. The protein bands are labeled K1 to K6 according to their molecular weight from 75,000 (K1) to 14,000 (K6). The polyvalent antiserum to granules recognizes most of the protein bands as determined by Western blotting analysis. Extraction of granules with 0.5 M phosphate buffer in the presence of protease inhibitors solubilizes the Ca-dependent cytolytic activity and allows its purification by gel-filtration and ion exchange chromatography using the MonoQ-fast protein liquid chromatography(FPLC) system (Fig. 26). Ca-dependent cytolytic activity resides in the 75,000 dalton protein corresponding to K1 in Figure 23. Incubation of the isolated protein with erythrocytes in the presence of Ca and subsequent analysis of the isolated membranes by negative staining electron microscopy shows the formation of membrane lesions corresponding to poly perforin 1 (Fig. 27). The K1 protein band thus corresponds to perforin 1 as defined by the original morphological criteria.

Functional Characterization of Perforin 1

Functional activity of isolated perforin 1 (P1) is dependent on Ca, which is required for P1 polymerization. Preincubation of P1 with Ca or with Zn inhibits

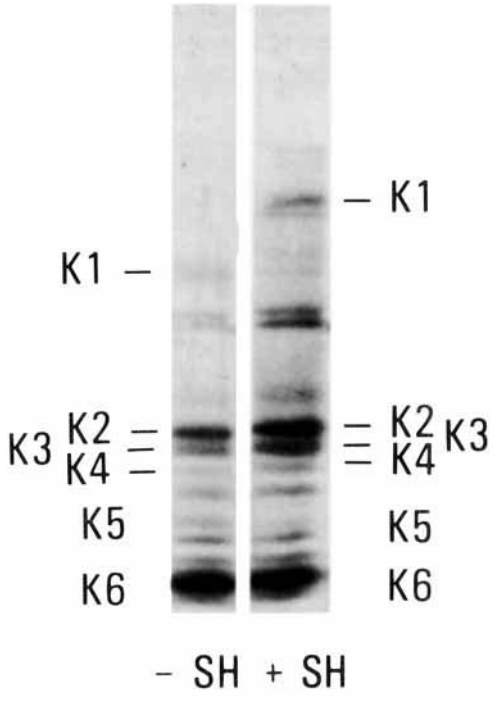

Fig. 25. Protein banding pattern on SDS-polyacrylamide gel electrophoresis of isolated CTLL2 granules. The bands are labeled K1 to K6 according to their molecular weight.

subsequent lysis of erythrocytes because preassembled complexes are incapable of inserting into target membranes. The metal dependence of P1 is similar but not identical to that of granules, suggesting that packaging of P1 in granules influences its properties to some extent. Both isolated perforin as well as granules are rapidly inactivated at 37°C in the presence of Ca and serum.

200 ng P1 lyse 2×10^8 erythrocytes with one effective hit per cell, corresponding to 400 poly P1 complexes assuming 20 subunits per complex. P1 is also effective in lysing tumor cells.

Comparison of Poly C9 and Poly P1

The studies summarized in this chapter show intriguing analogies, but also differences, between human C9 and murine P1 (Table V). Both proteins may be considered as killer proteins causing membrane destruction by polymerization in the membrane, displacing in the process membrane constituents and forming large, stable membrane pores. Polymerization of both proteins can be induced by Zn ions, resulting in inactive polymeric complexes. The inactivation is due to the inability of the polymeric complex to insert; insertion has to take place during polymerization. P1, in contrast to C9, is very sensitive to Ca ions, and polymerization is readily induced by low (0.1 mM) Ca concentrations. Although isolated C9 is also affected by Ca, its specific polymerizing unit is the C5b-8 complex, which operates even in the presence of EDTA. In addition, C5b-8 promotes C9 insertion into membranes into which isolated C9 cannot insert. The function of C5b-8 may be defined as C9 receptor,

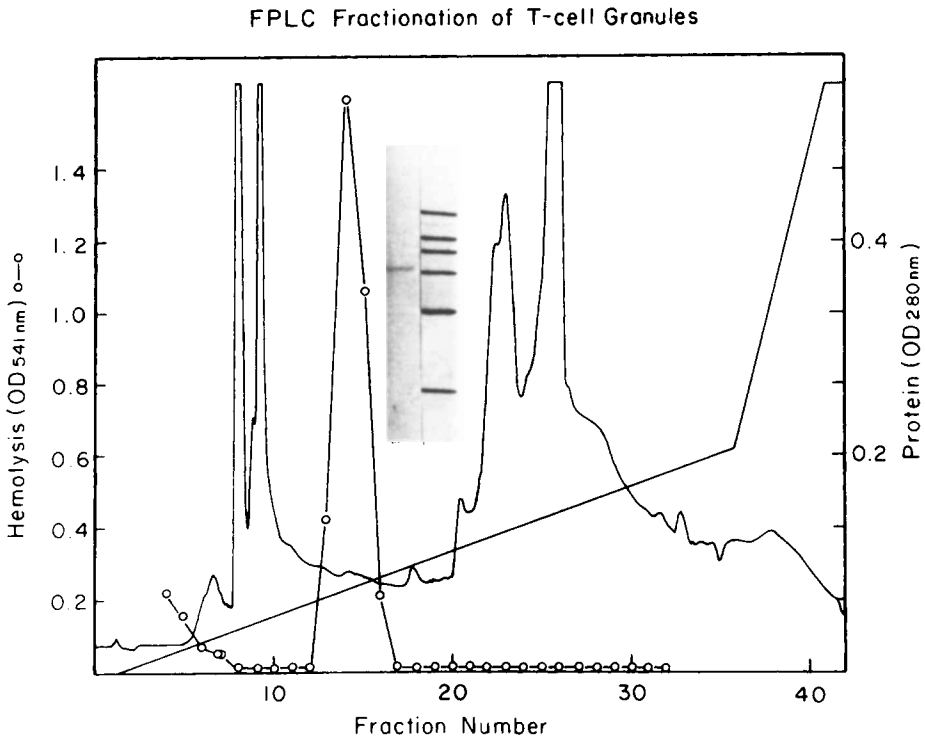

Fig. 26. FPLC purification of perforin 1 after salt extraction and gel-filtration of isolated granules. The inset shows the Coomassie blue staining of isolated P1 after Mono Qchromatography in comparison to markers. P1 migrates in the same position as K1 of intact granules (Fig. 24).

directing C9 to the target and accelerating polymerization and insertion. Complement thus first forms a receptor that is subsequently utilized to direct the killing event mediated by poly C9. The receptor (C5b-8) is incorporated into the killer unit in this process.

In the T-cell perforin system, there is no unit analogous to C5b-8 and thus no receptor directing P1 polymerization. Directionality of killing by CTL and NK cells probably is a function of the secretory process by which cytolytic granules are directed toward the target cell. The acceleration of P1 polymerization appears to be strictly a function of Ca ions and does not seem to be mediated by enzymatic action or physical association with other proteins. This mechanism is perfectly appropriate for cell-mediated killing, since Ca ions are sequestered from the cell interior or restricted to specific areas. During granule release perforins become exposed to Ca and undergo the polymerization reaction.

Perhaps the most interesting difference between C9 and P1 is the ability of P1 to insert into membranes without the help of a receptor complex. In contrast, C9 does not insert into biological membranes without C5b-8, even when it is induced to polymerize. The insertional efficiency of perforin 1 is not understood at present and requires more detailed information on the structure of P1 in comparison to C9.

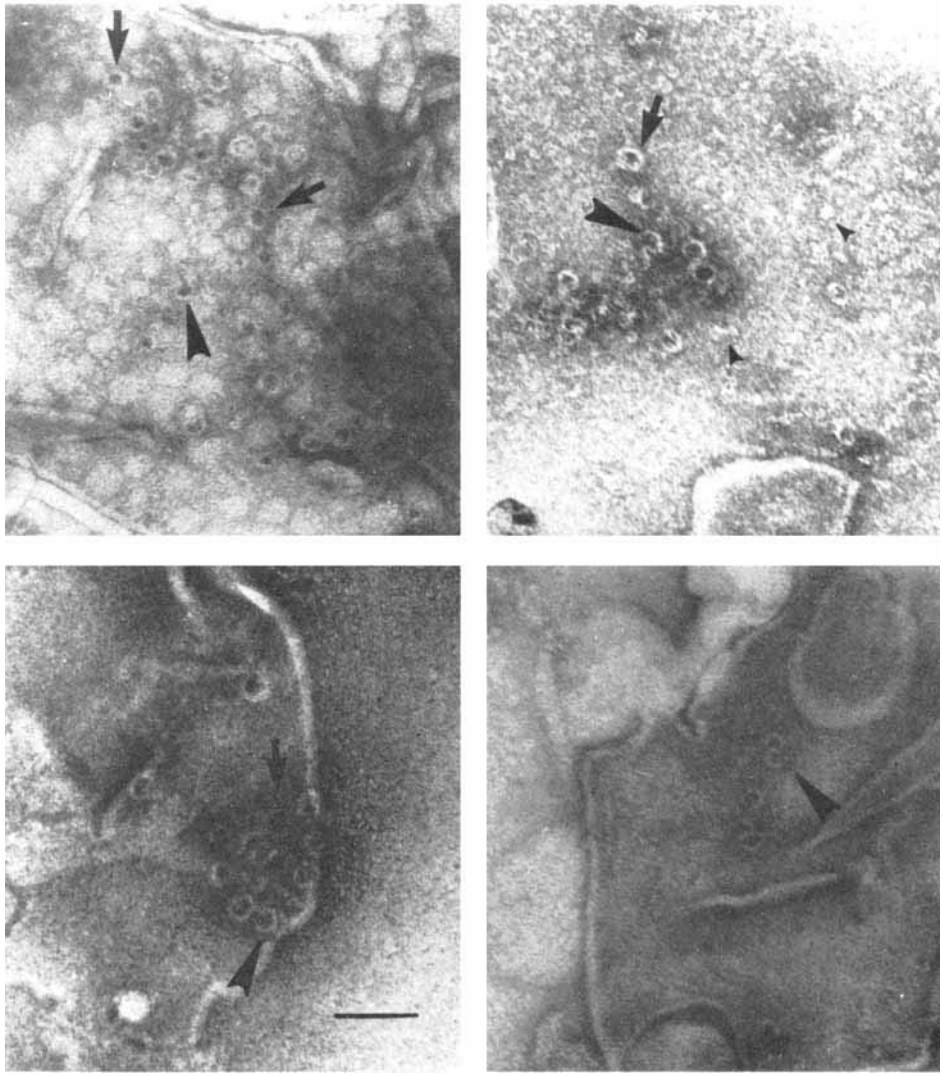

Fig. 27. Membrane lesions (poly perforin 1) formed on erythrocyte membranes by purified perforin 1 (P1) in the presence of CaC1 (all four panels). Scale bar: 800 Å.

Use of Transmembrane Pores for Entry of Toxic Molecules

In Figure 28 the steps leading to target lysis in complement and in the lymphocyte-mediated system are summarized. It is evident that the killing step shows analogies not only in the assembly of transmembrane tubules. The tubules in both systems are utilized for the entry of additional cytolytic molecules. In complement-mediated lysis of bacteria, lysozyme through the pores gains access to the peptidoglycan layer, resulting in the destruction of the cytoskeletal element of bacteria. In lymphocyte-mediated lysis of virus-infected or tumor cells, entry of nucleolytic

TABLE V. Comparison of Murine Perforin 1 With Human C9

	Perforin 1	C9
Molecular weight	73,000	73,000
Charge	Acidic	Acidic
Polymerization	Ca dependent	C5b-8 (metal independent)[a]
Ultrastructure of polymeric complex	Tubule, 160 Å long, 160 Å wide	Tubule, 160 Å long, 100 Å wide
SDS resistance	Yes	Yes
Function	Cytolysis	Cytolysis

[a]Zn dependent in the absence of C5b-8.

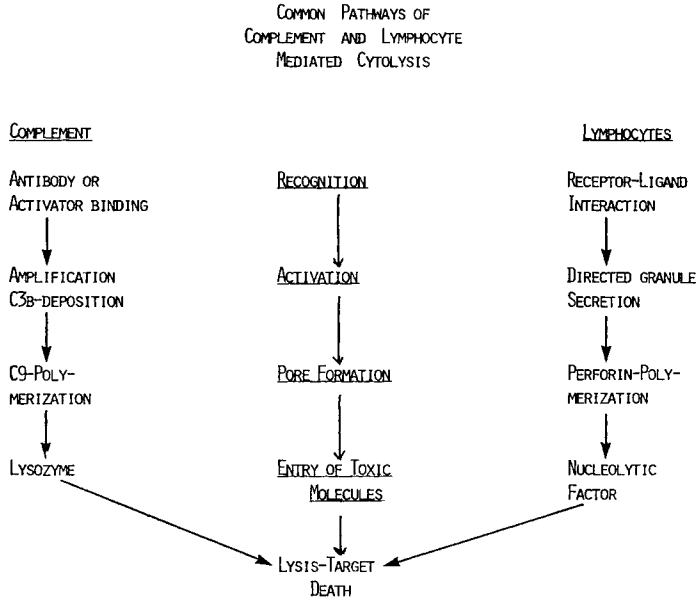

Fig. 28. Comparison of lytic pathways mediated by complement and by cytolytic lymphocytes.

factors through poly perforin pores causes target DNA degradation and destruction of potentially harmful genetic information in the target nucleus.

ACKNOWLEDGMENTS

I would like to thank Kristin Penichet for her excellent assistance.

Work conducted in this laboratory was supported by USPHS grants AI21999 and Ca 39201 and by a grant from the American Cancer Society (IM396).

REFERENCES

1. Podack ER, Tschopp J: Proc Natl Acad Sci USA 79:574, 1982.
2. Tschopp J: J Biol Chem 259:10569, 1984.

3. Podack ER, Tschopp J: J Biol Chem 257:15204, 1982.
4. Yamamoto K, Kawashima T, Migita S: J Biol Chem 257:8573, 1982.
5. Yamomoto K, Migita S: J Immunol 129:2335, 1982.
6. Yamomoto K, Migita S: J Biol Chem 238:7887, 1983.
7. Tschopp J, Engel A, Podack ER: J Biol Chem 259:1922, 1984.
8. Tschopp J, Muller-Eberhard HJ, Podack ER: Nature 298:534, 1982.
9. Young JDE, Cohn ZA, Podack ER:In Henkart P and Martz E (eds): "Mechanisms of Cell Mediated Cytoxicity." New York: Plenum Press (in press).
10. Podack ER, Tschopp J, Muller-Eberhard HJ: J Exp Med 156:268, 1982.
11. DiScipio RG, Gehring MR, Podack ER, Kan CC, Hugli TE, Fey GH: Proc Natl Acad Sci USA 81:7298, 1984.
12. Ishida B, Wisniewski BF, Levine CH, Esser AF: J Biol Chem 257:10551, 1982.
13. Stanley KK, Kocher HP, Luzio GP, Jackson P, Tschopp J: Embo J 4:375, 1985.
14. Yamamoto T, Davis CG, Brown MS, Schneider WY, Casey ML, Goldstein JL, Russel DW: Cell 39:27, 1984.
15. Biesecker G, Gerard C, Hugli TE: J Biol Chem 257:2584, 1982.
16. Podack ER: J Biol Chem 259:8641, 1984.
17. Tschopp J, Muller-Eberhard HJ, Podack ER: Proc Natl Acad Sci USA 79:7474, 1982.
18. Monahan JB, Stewart JL, Sodetz JM: J Biol Chem 258:5056, 1982.
19. Podack ER, Stoffel W, Esser AF, Muller-Eberhard HJ: Proc Natl Acad Sci USA 78:4544, 1981.
20. Hu VW, Esser AF, Podack ER, Wisnieski BJ: J Immunol 127:380, 1981.
21. Steckel EW, Welbaum BE, Sodetz JM: J Biol Chem 25:4318, 1983.
22. Tschopp J, Podack ER, Muller-Eberhard HJ: J Immunol 134:495, 1985.
23. Podack ER, Mueller-Eberhard HJ: J Biol Chem 256:3145, 1981.
24. Cheng KJ, Wiedmer T, Sims PJ: J Immunol 135:459, 1985.
25. Podack ER, Muller-Eberhard HJ: J Immunol: 124:332, 1980.
26. Rommel FA, Mayer MM: J Immunol 110:637, 1973.
27. Kolb WP, Muller-Eberhard HJ: J Immunol 113:479, 1974.
28. Sims PJ: Biochim Biophys Acta 732:541, 1983.
29. Ramm LE, Whiteow MB, Mayer MM: J Immunol 135:2594, 1985.
30. Ramm LE, Mayer MM: J Immunol 124:2281, 1980.
31. Podack ER, Biesecker G, Kolb WP, Muller Eberhard HJ: J Immunol 121:484, 1978.
32. Bhakdi S, Tranum-Jensen J: J Immunol 133:1453, 1984.
33. Stewart JL, Monahan JB, Brickner A, Sodetz JM: Biochemistry 23:4016, 1984.
34. Bhakdi S: Behring Inst Comm 65:1, 1980.
35. Biesecker G, Podack ER, Halverson CA, Muller-Eberhard HJ: J Exp Med 149:448, 1979.
36. Bhakdi S, Bhakdi-Lehnen B, Tranum-Jensen J: Immunol 37:901, 1979.
37. Bhakdi S, Tranum-Jensen J: Proc Natl Acad Sci USA 78:1818, 1981.
38. Bhakdi S, Tranum-Jensen J: Biochim Biophys Acta 737:343, 1983.
39. Rauterberg EW, Ungemach B, Gebest HJ: J Immunol 122:355, 1979.
40. Bauer J, Podack ER, Valet G: J Immunol 113:479, 1979.
41. Tranum-Jensen J, Bhakdi S: J Cell Biol 97:618, 1983.
42. Esser AF, Bartholomew RM, Muller-Eberhard HJ: Proc Natl Acad Sci USA 76:5843, 1979.
43. Esser AF, Kolb WP, Podack ER, Muller-Eberhard HJ: Proc Natl Acad Sci USA 76:1410, 1979.
44. Podack ER, Biesecker G,. Muller-Eberhard HJ: Proc Natl Acad Sci USA 76:897, 1979.
45. Bhakdi S, Tranum-Jensen J: Immunol 41:737, 1980.
46. Podack ER, Esser AF, Biesecker G, Muller-Eberhard HJ: J Exp Med 151:307, 1980.
47. Schreiber RD, Morrison DC, Podack ER, Muller-Eberhard HJ: J Exp Med 149:870, 1979.
48. Dankert JR, Esser AF: Proc Natl Acad Sci USA 82:2182, 1985.
49. Boyle MDP, Borsos T: J Immunol 123:71, 1979.
50. Boyle MDP, Gee AP, Borsos T: J Immunol 123:77, 1979.
51. Dalmasso AP, Benson BA: J Immunol 127:2214, 1981.
52. Giavedoni EB, Chow YM, Dalmasso AP: J Immunol 122:240, 1979.
53. Ramm LE, Whitlow MB, Mayer MM: J Immunol 129:1143, 1982.
54. Ramm LE, Whitlow MB, Mayer MM: Proc Natn acad Sci USA 79:4751, 1982.
55. Podack ER, Esser AF, Biesecker G, Muller-Eberhard HJ: J Exp Med 151:301, 1980.
56. Podack ER, Kolb WP, Muller-Eberhard HJ: J Immunol 120:1841, 1978.

57. Preissner K, Podack ER, Muller-Eberhard HJ: J Immunol 135:452, 1985.
58. Preissner K, Podack ER, Muller-Eberhard HJ: J Immunol 135:445, 1985.
59. Stolfi RL: J Immunol 100:46, 1968.
60. Lachmann PH, Thompson RA: J Exp Med 131:643, 1970.
61. Gotze O, Muller-Eberhard HJ: J Exp Med 132:898, 1970.
62. Lint TF, Behrends CL, Gewurz H: J Immunol 119:883, 1977.
63. Nemerow GR, Yamamoto KI, Lint TF: J Immunol 123:1245, 1979.
64. Podack ER, Kolb WP, Muller-Eberhard HJ: J Immunol 120:1841, 1978.
65. Podack ER, Preissner KT, Muller-Eberhard HJ: Acta Pathol Microbiol Immunol C92, S284:89, 1984.
66. Haensch GM, Hammer CH, Vanguri P, Shin ML: Proc Natl Acad Sci USA 78:5118, 1981.
67. Rosenfeld SI, Packman CH, Leddy JP: J Clin Invest 71:795, 1984.
68. Berke G: Immunol Rev 72:5, 1983.
69. Brooks CG, Uvolal DL, Henney CS: Immunol Rev 72:43, 1983.
70. Martz E, Heagy W, Gromkowski SH: Immunol Rev 72:73, 1983.
71. Russel JH: Immunol Rev 72:97, 1983.
72. Bonavida B, Bradley T, Fan J, Hiserodt J, Effros R, Wexler H: Immunol Rev 72:119, 1983.
73. Podack ER, Konigsberg PJ: J Exp Med 160:695, 1984.
74. Millard PH, Henkart MP, Reynolds CW, Henkart PA: J Immunol 132:3197, 1984.
75. Sanderson CY: Biol Rev 56:153, 1981.
76. Duke RC, Chervenak R, Cohen JJ: Proc Natl Acad Sci USA 80:6361, 1983.
77. Dourmashkin RR, Deteix P, Simone CB, Henkart PA: Clin Exp Immunol 42:554, 1980.
78. Podack ER, Dennert G: Nature 302:442, 1982.
79. Dennert G, Podack ER: J Exp Med 157:1483, 1983.
80. Podack ER, Young JDE, Cohn ZA: Proc Natl Acad Sci USA 1985 (in press).
81. Podack ER, Konigsberg PJ, Acha-Orbea H, Pircher H, Hengartner H: In Henkart P and Martz E (eds): "Mechanisms in Cell Mediated Cytoxicity II. New York: Plenum Publishing, 1985, pp 99–119.
82. Podack ER: Immunol Today 6:21, 1985.
83. Kupfer A, Dennert G, Singer SJ: Proc Natl Acad Sci USA 80:7224, 1983.
84. Geiger B, Rosen D, Berke G: J Cell Biol 95:137, 1982.
85. Russel JH, Masakowski VR, Dobos CB: J Immunol 124:1100, 1980.
86. Konigsberg PJ, Podack ER: J Leukocyte Biol 38:109, 1985.
87. Schmid DS, Tite JP, Ruddle NH: Personal communication.
88. Ruddle NH: Immunol Today 6:156, 1985.
89. Aggarwal BB, Moffat B, Havkins RN: J Biol Chem 259:686, 1984.
90. Carswell EA, Old LJ, Kassel RL, Green S, Fiore N, Williamson B: Proc Natl Acad Sci USA 72:3666, 1975.
91. Ruddle NH, Waksman BH: J Exp Med 128:1267, 1968.
92. Granger GA, Kolb WP: J Immunol 101:111, 1968.
93. Wright SC, Hiserodt JC, Bonavida B: Trans Proc 13:770, 1981.